# Identifying sources and distribution of organic pollutants in a Moroccan river: Characterization of dissolved organic matter by absorption, excitation–emission fluorescence and chemometric analyses

Hassan Ba-Haddou, Omar Taoussi, Saadia Ait Lyazidi, Marina Coquery, Matthieu Masson, Mustapha Haddad, Abdelmajid El Bakkali, Christelle Margoum

Journal of Hazardous Materials 480 (2024) 135899

Contents lists available at ScienceDirect

Journal of Hazardous Materials

journal homepage: www.elsevier.com/locate/jhazmat

# Identifying sources and distribution of organic pollutants in a Moroccan river: Characterization of dissolved organic matter by absorption, excitation–emission fluorescence and chemometric analyses

Hassan Ba-Haddou [a,b,*], Omar Taoussi [a,c], Saadia Ait Lyazidi [a], Marina Coquery [b], Matthieu Masson [b], Mustapha Haddad [a], Abdelmajid El Bakkali [a], Christelle Margoum [b]

[a] University of Moulay Ismail – Faculty of Sciences, LASMAR, URL-CNRST, No. 7, Meknes, Morocco
[b] INRAE, UR RiverLy, 69625 Villeurbanne, France
[c] Université de Sherbrooke, Department of Civil and Building Engineering, Environmental Engineering Laboratory, Sherbrooke, QC, Canada

## HIGHLIGHTS

- Characterization of DOM in water from groundwater, surface waters and WWTP effluents.
- Exploring DOM by coupling UV-Vis absorption, EEM fluorescence, and chemometrics.
- Assessment of wastewater treatment in lagoons using low-cost analytical techniques.
- Tracking sources and gradient of organic pollutants along the river.

## GRAPHICAL ABSTRACT

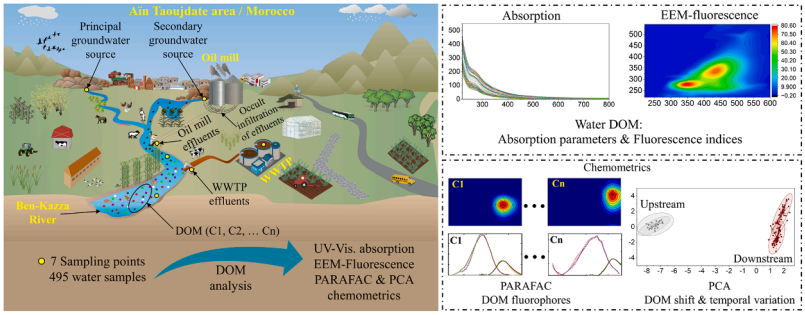


## ARTICLE INFO

*Keywords:*
Wastewater
WWTP
Contamination
Anthropogenic
PARAFAC-PCA

## ABSTRACT

This study investigates surface water contamination of Ben-Kazza River in Morocco, fed by effluents from an adjacent lagoon-based wastewater treatment plant (WWTP) and seasonally by industrial effluents, and which occasionally serves to irrigate agricultural fields. This study has two purpose: i) to track the main sources of contamination through the evolution of dissolved organic matter (DOM) characteristics along the watercourse, and ii) to characterize the WWTP influents and effluents with a focus on the efficiency of the lagoon treatment. We characterized a total of 495 water samples across the watercourse and from the inlet and outlet of the WWTP, using UV–visible absorption and excitation–emission fluorescence coupled with chemometric analyses. Absorption indicators and fluorescence indices were calculated and compared across sampling points. Results highlight spatial shifts together with temporal changes in DOM. PARAFAC identified components that varied between protein-like, humic-like and anthropogenic-like fluorophores along the river, permitted to trace the anthropogenic components and their sources. The lagoon treatment appeared to better remove fresh organic material than humic material: fluorescence intensity decreased by 68 % for peak T1 and by 22 % for peak C. Maximum fluorescence intensities (Fmax) decreased across all PARAFAC components, leading to more than 55 % reduction of ΣFmax.

* Corresponding author at: University of Moulay Ismail – Faculty of Sciences, LASMAR, URL-CNRST, No. 7, Meknes, Morocco.
*E-mail addresses:* hassan.bahaddou@edu.umi.ac.ma, hassan.ba-haddou@inrae.fr, hassanbahaddou37@gmail.com (H. Ba-Haddou).

https://doi.org/10.1016/j.jhazmat.2024.135899
Received 29 May 2024; Received in revised form 9 September 2024; Accepted 17 September 2024
Available online 18 September 2024

## 1. Introduction

In Morocco, over the last few decades, water resources controls have been increased to manage the country's water supply while taking local needs into account. With this in mind, interest in water recycling is growing rapidly; it is aimed to mobilize 325 million $m^3$ of treated water by 2030, mainly to help irrigate cropland exposed to limited freshwater resources [1]. Hence, monitoring surface waters subjected to effluent discharges is being increasingly required. Entrapment of anthropogenic micropollutants by water organic matter (OM), via a variety of molecular interactions [2,3], increases their solubility, weight, and hydrophilicity [4]. However, even after treatment, WWTP effluents still contain a substantial OM load. Consequently, the rate of removal of OM fractions is among the indicators of water treatment efficiency [5].

Dissolved organic matter (DOM), which constitutes the bulk of water OM, includes humic acids, fulvic acids, carbohydrates and amino acids. It plays key roles in controlling the fate of environmental pollutants and the biogeochemistry of organic carbon in the global ecosystem [6–8]; consequently, determining the types and origins of DOM fractions in waters has become a growing concern worldwide. In this sense, fluorescent dissolved organic matter (FDOM), which is the fraction of DOM that absorbs and emits light over a broad range of ultraviolet–visible wavelengths, is a surrogate for tracking changes in water OM content [9–12]; and the relative distributions of different fluorescent components could help to distinguish DOM sources [13]. In natural water and wastewater science, sophisticated techniques such as Fourier-Transform Infrared Spectroscopy (FTIR), Nuclear Magnetic Resonance (NMR) and Liquid Chromatography/Mass Spectrometry (LC/MS) usually require laborious and time-intensive procedures [14–17]. However, excitation–emission fluorescence and 'Parallel Factor Analysis' (PARAFAC) chemometrics is increasingly being used to monitor and study the dynamics of DOM [18]. Fluorescence excitation–emission matrices (EEM) is a rapid, relatively inexpensive and highly sensitive tool for characterizing the DOM components found in water systems [19,20].

The aim of the present research was to i) to track the main sources of contamination through the evolution of DOM characteristics along the Ben-Kazza River, where it crosses the commune of Aïn Taoujdate in Morocco, and ii) monitor the performance of the WWTP adjacent to and feeding into the watercourse. The analytical approach adopted to track DOM changes throughout the river is based on EEM fluorescence combined with UV–visible absorption, and supported by PARAFAC chemometrics and principal component analysis (PCA). Indeed, fluorescence/absorption/chemometrics-based metrics has several advantages over other chromatographic analyses techniques in the continuous monitoring of waters and wastewaters [9,21–23]. Firstly, EEM provides a comprehensive characterization of dissolved organic matter (DOM) based on its fluorescence properties, allowing for the identification of various fluorescent components. This method can effectively distinguish between different types of organic matter, such as protein-like, humic-like, and anthropogenic-like fluorophores, providing valuable information about the sources and nature of contaminants. Secondly, UV-Vis absorption spectroscopy offers a rapid and cost-effective way to quantify the concentration of organic compounds in water samples. It provides information about the absorbance of organic matter at different wavelengths, allowing for the identification of specific organic compounds. Additionally, PARAFAC analysis, when combined with EEM, allows for the decomposition of EEM data into individual fluorophores, enabling a more detailed and accurate characterization of DOM compared to traditional chromatographic methods. Combined with PCA, it also facilitates the tracking of spatial and temporal changes in DOM components. Moreover, the rapidity, reliability and versatility of techniques make them suitable for routine monitoring of water quality and pollutant assessment in complex environmental samples such as drinking waters and wastewaters.

A previous study [24] attempted to characterize DOM quality and quantity in raw sewage waters of the Seine Centre WWTP (France), aiming to better control the biological treatment process and reduce energy costs at the WWTP. However, despite the richness and reliability of this laboratory investigation, the approach adopted, based on empirical relationships between BOD5 and fluorescence parameters, including PARAFAC components along with HIX and BIX indices, seems complex and difficult to apply at real scale for WWTPs. Also, such an approach required a conceptual mathematical model to describe relationships between fluorescence indices, absorption indicators, and conventional global quality parameters of sewage water. Another recent study [25] used EEM/PARAFAC fluorescence analysis to study the geographical and spatial variations of fluorescence signal along the Gapeau River (France), from upstream of a WWTP to the coastal waters, and to evaluate the impact of effluent wastewaters on the river DOM. However, this investigation did not consider either absorption measurements to control the internal filter effect, or fluorescence indices to enrich the fluorescence measurements. Therefore, the adopted EEM/-PARAFAC fluorescence approach could be improved by reconsidering the experimental parameters to obtain reliable information on the spatial and temporal variations of river DOM. The present work, which is combining absorption, fluorescence and chemometric analyses, aims to enrich experimental studies to monitor chromophoric/fluorescent DOM in river waters.

## 2. Materials and methods

### 2.1. Study area

The commune of Aïn Taoujdate is part of the province of El Hajeb in the Fez–Meknes region in Morocco, located about 20 km from Fez and 50 km from Meknes (Fig. 1). This commune, characterized by a semi-arid sub-continental climate and covering an area of 11 $km^2$ with an average altitude of 465 m, has an estimated population of approximately 40,000 people whose activity consists mainly in farming and livestock. The Ben-Kazza River springs from Ben-Kazza source (33°57'06.3"N 5°12'55.9"W) and flows through the Aïn Taoujdate area towards Mikkes River, part of the Sidi Echahed dam watershed.

As shown in Fig. 1, there is a WWTP installed in the area of Aïn Taoujdate (at 33°58'17.1"N 5°13'30.7"W), and an olive oil production facility adjacent to the watercourse (at 33°57'06.3"N 5°13'10.1"W). These two installations discharge their effluents into the Ben-Kazza River, while the downstream water flow is used to irrigate agricultural fields in times of drought and to provide water for livestock [26]. The WWTP, covering an area of 10 ha, is a natural lagoon model based on a series of anaerobic ponds. Its treatment capacity is about 1500 $m^3$ per day, for an estimated pollutant load of approximately 700 kg of biochemical oxygen demand (BOD5) per day. The WWTP is fed by an inlet pipe carrying domestic and urban wastewaters from Aïn Taoujdate city community. The agro-industrial oil mill processes olives, soybeans or sunflower seeds depending on the season, and discharges its partially treated effluents into the Ben-Kazza River. In addition to these two sources of pollution, run-off from agricultural activity is another diffuse source of pollution. This combination of industrial activity, WWTP effluent and natural runoff obviously compromises the natural environmental compartments of the Aïn-Taoujdate area [26].

### 2.2. Sampling

In order to follow the pollution gradient along Ben-Kazza River, sampling was carried out at seven points (P1 to P7) along the river over a distance of 2.79 km from the river's source (P1). Fig. 1 maps these sampling points along with their spatial coordinates.

The source of the river (P1), which is located far upstream from the various sources of contamination flowing into the watercourse, is considered as a reference. P2 is a secondary groundwater source that seems receiving infiltrations from the oil mill's marginal storage tanks. P3 is a discharge point for effluents from the industrial oil mill facility.

P4 is a first confluence point where waters from P1, P2 and P3 meet. P5 and P6 represent respectively the influent and effluent zones of the WWTP. P7 is an overall confluence point where all the waters received into the Ben-Kazza River meet.

As the hydraulic residence time of the WWTP is 14 days [26], A first series of two campaigns was conducted 14 days apart in March and April 2022; and a second series of two campaigns, also conducted 14 days apart, was conducted in May and June 2022. The aim of these campaigns was to monitor OM removal between the WWTP inflow and outflow and to track the spatial and temporal changes in DOM throughout the river from the upstream source (P1) to the downstream confluence zone (P7). A total of 495 water samples were collected, as a relevant sampling program allows for better chemometric analysis [27,28].

### 2.3. Sample preparation

Water samples were collected into 30 mL amber glass vials that had been cleaned and oven-dried 200 °C for 4 h. Immediately after sampling, the vials were placed in a light-shielded cooler at approximately ± 4 °C, and then transported to the laboratory and placed in refrigerated storage at 4 °C. The following day, the water samples were filtered through 0.7 µm pore-size Whatman GF/F filters using a borosilicate glass syringe with a stainless steel membrane holder. Analysis began immediately after filtration, and continued for approximately ten days. Under these storage conditions, water can remain stable for up to 59 days without undergoing any changes that would interfere with the intended spectrometric measurements [29].

The pH values measured in the different waters were around 7.5, except in samples from points P2 and P3 in which they were close to 8.6. These higher pH levels do not cause major distortions in absorption or fluorescence spectra [30]; pH values between 5 and 9 have generally shown relatively small differences in UV absorption [31].

### 2.4. Environmental parameters

We monitored the meteorology of the Aïn Taoujdate area throughout the sampling period. Indeed, rainwater can transfer organic compounds from the atmosphere to surrounding environments [32] and high temperatures can induce changes in the properties of water OM [33]; also, dissolved organic matter (DOM) in surface waters can vary with seasonal variations in rainfall intensity, UV radiation, and temperature [34]. Based on meteorological data from the Meteoblue service, there was almost no precipitation, and temperatures fluctuated around 15 °C [35] (Fig. S1). Under these conditions, organic material in the sampled water cannot be subject to rainfall or temperature-induced changes.

### 2.5. DOM characterization methods: analytical techniques

Dissolved organic carbon (DOC) concentrations in filtered samples were determined using the high-temperature catalytic combustion method according to standard NF EN 1484 [36]. The analysis was performed using a multi N/C® model 3100 Analytik Jena TOC analyzer. Each measure was repeated three times and averaged. These measurements were carried out on samples from the second campaign.

Absorbance measurements on filtered water samples were recorded on a Jasco UV/VIS/NIR V-570 spectrophotometer in the 200–800 nm spectral range using a 1 cm optical path quartz cell and Milli-Q ultrapure water as a reference blank. The absorption indicators (specific ultraviolet absorbance at 254 nm (SUVA), E2/E3, E2/E4, S275–295, S350–400 spectral slopes and slope ratio) used in this study are described in Table 1.

The EEM-fluorescence were generated using a Shimadzu RF-5301PC

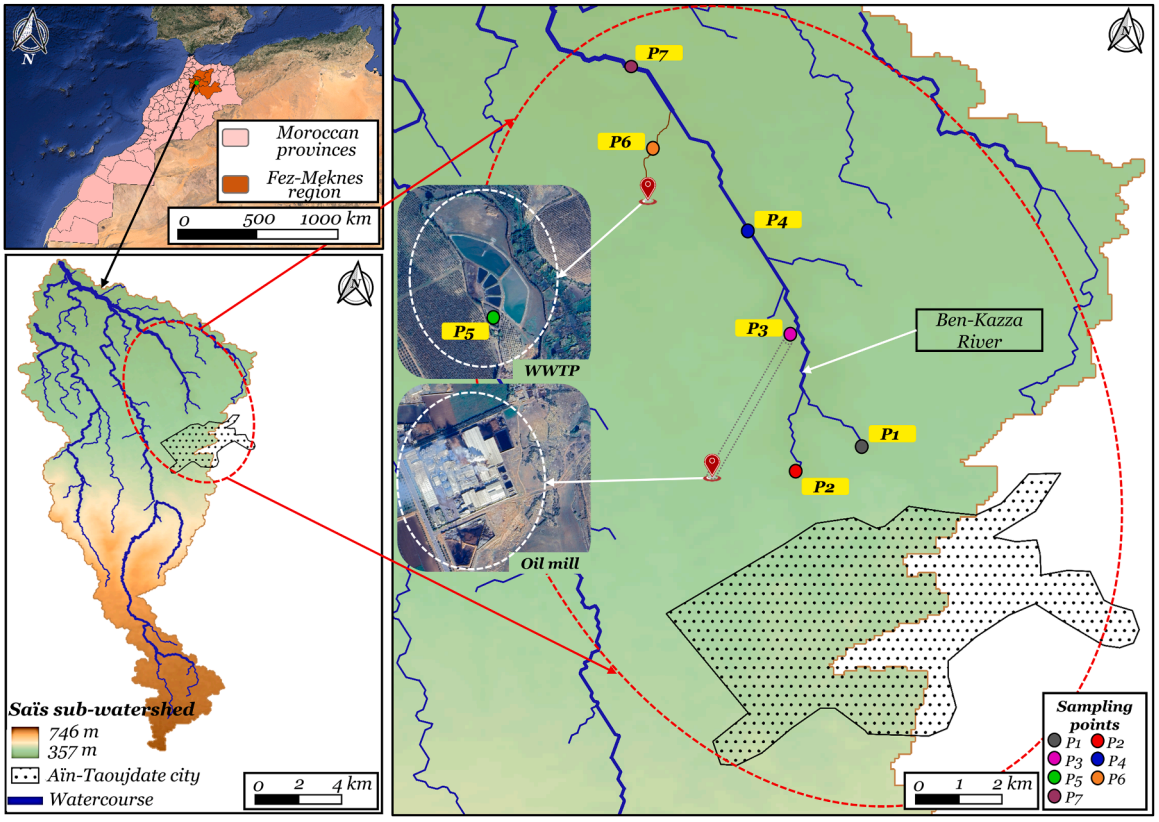


**Fig. 1.** Study area (Aïn-Taoujdate city) and sampling sites along the Ben-Kazza River. P1 (33°57'06.3"N 5°12'55.9"W), P2 (33°57'08.8"N 5°12'59.2"W), P3 (33°57'27.6"N 5°12'59.3"W), P4 (33°57'39.6"N 5°13'01.3"W), P5 (33°58'14.2"N 5°13'32.6"W), P6 (33°58'11.3"N 5°13'27.4"W) and P7 (33°58'30.6"N 5°13'42.9"W).

spectrofluorometer equipped with a xenon lamp, using a 1 cm optical path quartz cell and a high-sensitivity sample holder. For all water samples, 5 nm/5 nm slits were used in both excitation and emission, except for samples collected at site P1 for which 10 nm/10 nm slits were used. The matrices were recorded at 5 nm increments in the 220–550 nm spectral range in excitation, and at 1 nm increments in the 220–600 nm spectral range in emission. In order to avoid any internal filter effect that would compromise the fluorescence intensities, the samples were diluted until absorbance neared 0.05 at 254 nm [55]. In addition, EEMs of pure deionized water were obtained for each day of measurements. Each sample required 67 excitation–emission scans, and each EEM required a time of 23 min overall. The EEMs were generated using the Lab-Solution software controlling the spectrometer. In order to refine the interpretation of the fluorescence results, we used three indices in this study: fluorescence index (FI), biological index (BIX), and humification index (HIX). Descriptions of these indices can be found in Table S1.

### 2.6. Creation of a fluorescence database

Given the prevalence of anthropogenic organic pollutants in aquatic environments, and particularly wastewater, identifying them in environmental samples using EEM/PARAFAC fluorescence remains hard due to the superposition of multiple fluorescence foci. To solve this problem, we previously established a database using EEM fluorescence data for 108 micropollutants [56]. The main objective is to facilitate EEM/-PARAFAC fluorescence-based identification of micropollutants belonging to hormones, pharmaceuticals and pesticides families providing researchers with a catalog of valuable fluorometric spectral fingerprints. That encloses information on excitation and emission properties over a wide optical spectral range. This database constitutes a user-friendly tool for exploring the fluorescence landscapes of environmental matrices. These landscapes are often hard to interpret (as was the case here) due to the strong fluorescence of the OM, and to micropollutants emitting in nearby spectral regions.

### 2.7. Chemometric analysis

PARAFAC, is a data decomposition algorithm. It consists in decomposing experimental fluorescence EEMs into individual sub-matrices corresponding to the fluorophores coexisting in the analyzed samples. This multivariate analysis method is applicable to datasets arranged in 3rd-order arrays (in the case of fluorescence data) that cross-reference the three data inputs: sample, excitation wavelength, and emission wavelength [57,58].

The algorithm consists in a trilinear decomposition of a data cube according to Eq.1:

$$x_{ijk} = \sum_{f=1}^{F} = a_{if} b_{jf} c_{kf} + \varepsilon_{ijk} \quad (1)$$

where i = 1, 2 … I, j = 1, 2 … J, k = 1, 2 … K, and I, J and K designate the numbers of samples, emission wavelengths and excitation wavelengths, respectively.

$x_{ijk}$ is the fluorescence intensity of sample *i* for the pair of excitation and emission wavelengths j, k. *F* is the number of components in the model, i.e. the presumed number of the fluorophores coexisting in the samples analyzed, $a_{if}$ is directly proportional to the concentration of fluorophore *F* in sample *i*, defined by the scores, while $b_{jf}$ and $c_{kf}$ are estimates of the emission and excitation spectra for component f, defined as loadings. $\varepsilon_{ijk}$ is the variance not accounted for by the model, i.e. the residual signal [59,60]. An example of PARAFAC decomposition is shown in Fig. S3. PARAFAC chemometric analysis is widely used in water and soils monitoring [61,62].

The experimental fluorescence matrices acquired for all samples

**Table 1**
UV–visible absorption indicators for DOM and their descriptions.

| Parameter | Description and indication | References |
|---|---|---|
| Absorbance at λ = 355 nm (Abs355) | – Abs355 increases significantly as water quality deteriorates.<br>– Abs355 indicates that the concentration of dissolved organic matter progressively increases with decreasing water quality. | [37,38] |
| Specific UV absorbance at 254 nm, SUVA254 (L.mg$^{-1}$.m$^{-1}$) | – SUVA254 is calculated by normalizing the UV absorbance at a 254 nm wavelength to the concentration of dissolved organic carbon (DOC). It is an indicator of the aromaticity of organic matter, providing a general quantitative estimate of aromatic content per unit concentration of carbon.<br>– SUVA254 is positively correlated with the aromaticity of CDOM<br>– Waters with high SUVA254 values, i.e. ≥ 4 L.mg−1.m$^{-1}$, have a high content of complex heterogeneous aromatic-rich macromolecular organic compounds<br>– Waters with low SUVA254 values, i.e. ≤ 3 L.mg−1.m$^{-1}$, predominantly contain homogeneous aromatic-poor low-molecular-weight materials. | [39–43] |
| $E_{2/3} = A_{250} / A_{365}$ | – Negatively related to protein-like DOM as proteins contain significantly fewer aromatic rings than humic substances.<br>– Calculated as the ratio of absorbance between 250 and 365 nm.<br>– It is an indicator of the degree of humification of organic matter in water, and can also indicate the source of the organic matter.<br>– E2/E3 serves to track the changes in the relative size of organic matter molecules; it is inversely correlated with the molecular size of DOM.<br>– When E2/E3 < 3.5, it mainly reflects the absorption characteristics of larger organic molecules such as humic acid.<br>– When E2/E3 > 3.5, it mainly reflects the absorption characteristics of smaller organic molecules, such as fulvic acid. | [44–46] |
| $E_{2/4} = A_{254} / A_{436}$ | – Calculated as the ratio of absorbance at 254 nm to absorbance at 436 nm,<br>– E2/E4 values in the range 4–11 are indicative of terrestrial DOM.<br>– Median E2/E4 values in the range 11–30 are indicative of DOM derived mostly from microbial sources.<br>– The smaller the E2/E4 value, the greater the degree of condensation of organic molecules. | [47–50] |
| $S_{275/295}$ nm$^{-1}$ and $S_{350/400}$ nm$^{-1}$ | – Means that the slopes of the straight-line natural logarithm of the absorbance spectra fit between 275 and 295 nm and 350 and 400 nm.<br>– Used to characterize the ratio of fulvic acid to humic acid.<br>– Higher *S* values typically indicate low-molecular-weight material and/or decreasing aromaticity<br>– Generally increases on irradiation. | [50–52] |
| $SR = \frac{S275/295}{S350/400}$ | – Waters with SR < 1 are predominately terrigenous and rich in high-molecular-weight organic matter. | [52–54] |

(continued on next page)

**Table 1** (*continued*)

| Parameter | Description and indication | References |
|---|---|---|
| | – Waters with SR > 1 are predominately rich in fresh microbial and low-molecular-weight organic matter | |

collected at each sampling point during the two campaigns were processed by PARAFAC. Here, PARAFAC modeling was performed in MATLAB® R2020a using the DrEEM 0.6.0 toolbox [57]. The pre-processing step comprised blank subtraction, Raman normalization, smoothing and cutting of the Rayleigh and Raman scatter lines [57].

Models ranging from 2 to 9 components were used to assess the presence of the appropriate fluorophores in the samples from each sampling point. The most suitable model was selected based on the sum of squared residuals and core consistency, which decreases progressively with increasing the number of components. Split-half validation was applied to set the number of PARAFAC components [57] that was determined as the highest number that enabled validation of all compared splits.

Outliers encompassing outlier samples or wavelengths [63] were excluded from processing in this study; this enables the PARAFAC model to calculate the maximum fluorescence intensity (Fmax) for each component using the standardized N-way toolbox for quantitative data [57]. These Fmax values then served to quantify components.

Factors of similarity between components were calculated using Tucker's congruence coefficient (TCC) according to the formula (Eq.2):

$$TTC(x,y) = \frac{\sum x_i y_i}{\sqrt{\sum x_i^2 \sum y_i^2}} \quad (2)$$

where TTC (x,y) is the congruence coefficient and $x_i$ and $y_i$ are the excitation or emission loadings of the two PARAFAC components to be compared [64]. According to [59], the component similarity factor is calculated as the product of the excitation loading similarity $TCC_{Ex}$ and the and emission loading similarity $TCC_{Em}$ (Eq.3)

$$mTCC = \quad TCC_{Ex} * \quad TCC_{Em} \quad (3)$$

This similarity factor metric *mTCC* ranges from 0 to 1 from completely different components to identical components [65,66].

Principal component analysis (PCA) was performed on the fluorescence and absorption data using OriginPro® 2024 software.

## 3. Results and discussion

### 3.1. Dissolved organic carbon

Monitoring the DOC gradient along the Ben-Kazza River highlighted the variability of waters feeding this watercourse, i.e. industrial discharges, WWTP effluents, and agricultural runoff. Table 2 reports the average DOC levels measured at all sampling points.

The DOC concentrations were perfectly consistent with the positions and characteristics of the various sampling points: the lowest DOC concentration was observed at the source P1 located far upstream where the water is clean, whereas the highest DOC concentrations were found at P2 and P3 where the water is charged with oil mill effluents. Oil mill wastewaters contain high levels of organic content, oil and grease, fatty acids, sulfates, phosphates, and phenolic chemicals [67,68]. The DOC content observed for site P4 can be explained by its proximity to point P3 and the dilution due to water flow from P1. The DOC concentrations at points P5 and P6 were respectively 150 and 29 mg/L, consistently with their respective positions upstream and downstream of the WWTP. The DOC content then decreased at the final sampling point P7; this can be explained either by dilution of the charged waters far from the sources of contamination, or by the photobleaching and mineralization induced by exposure to sunlight [69]. On other side, aver all sampling points the conductivity variation seems in concordance with this DOC gradient (Table 2).

### 3.2. UV–visible DOM characterizing

To gain insights into the DOM composition gradient across the Ben-Kazza River and to track its changes between the wastewater treatment plant (WWTP) influents and effluents, we studied key parameters based on UV-Visible absorption measurements. Fig. 2 shows the UV–visible absorption spectra measured on all sampled waters.

#### 3.2.1. Absorbance spectra

The absorbance spectra measured here showed similarities to absorbance spectra described in previous studies involving natural waters [70] and typical urban wastewaters [70,71]. The absorption spectrum corresponding to water source P1 is characteristic of natural waters, with the band around 300 nm due to the humic material [72] and the peak below 230 nm due to the inorganic chemicals present in natural waters [70,73]. The other sampling points encompassed a broad range of organic material spanning protein-like, detergent-like and human urine-like chromophores, while sampling points P2 to P6 also included colored chromophores absorbing at around 500 and 600 nm. This DOM absorbance variability across the sampling points manifested quantitatively in the absorption coefficient at 355 nm that increased significantly as water quality deteriorated (Fig. 3.f). High absorbance at this wavelength is generally associated with high levels of organic material; it is often related to chromophoric dissolved organic matter (CDOM) content in water and water quality [38].

The P3, P4 and P7 sampling points showed a more particular pattern, as the collected absorption spectra led to two different sets of spectra. This is not surprising, as all these sampling points are connected to the oil-mill effluents, which almost certainly carried different feedstock materials processed by the oil mill between the first and the second sampling campaigns. On another side, the spectra measured on the water samples collected at the point downstream of the WWTP (P6) showed a strong drop in absorbance compared to spectra measured on water samples collected at the upstream point (P5), which is consistent with the observed decrease of DOC between points P6 and P5, as shown above. The removal of suspended solids by settling during natural lagoon treatment removed absorbing organic materials from the wastewaters.

#### 3.2.2. Absorption indicators: SUVA, absorbance ratios, spectral slopes and slope ratios

To ascertain differences in the aromatic quality of the flow of water in the river through all sampling points, we calculated specific UV

**Table 2**
Physico-chemical parameters measured at the sampling points along the river.

| Sampling point | P1 | P2 | P3 | P4 | P5 | P6 | P7 |
|---|---|---|---|---|---|---|---|
| DOC (mg/L)* | 1.9 ± 0.2 | 100 ± 10 | 160 ± 20 | 39 ± 5 | 150 ± 20 | 29 ± 3 | 18 ± 2 |
| Conductivity (µS/cm) | 470 | 1750 | 2210 | 1570 | 2235 | 1910 | 1880 |
| Flow rate (L/s) | 149.5 | 24.8 | 5.7 | 164.6** | 76.4** | 49.0 | 207.7** |
| Flow velocity (m/s) | 0.68 | 0.83 | nd | 0.94 | 1.62 | 1.08 | 0.20 |

* (mean ± standard deviation, n = 3). * * approximate value. nd: not determined.

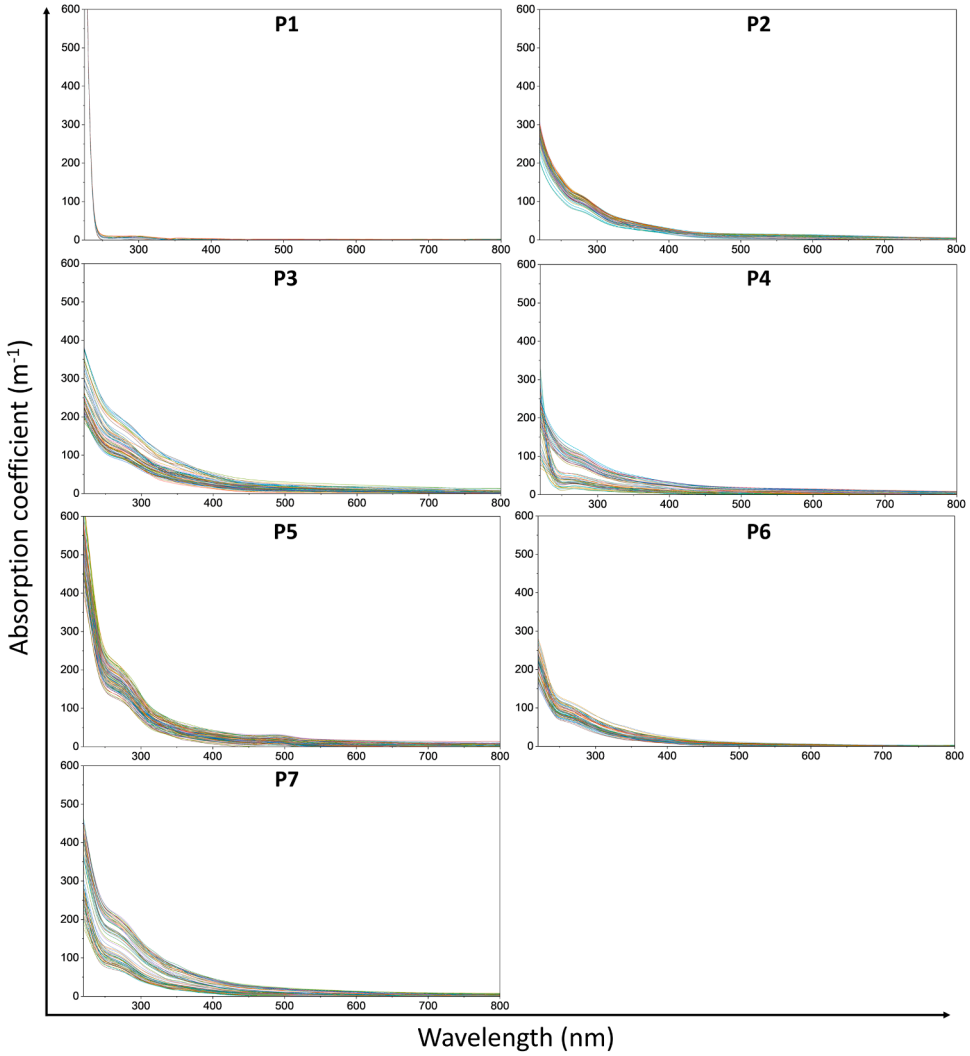


**Fig. 2.** UV-Vis absorption spectra of the water samples collected along the Ben-Kazza River. P1 (n = 20), P2 (n = 55), P3 (n = 80), P4 (n = 80), P5 (n = 90), P6 (n = 80) and P7 (n = 90). (n = number of samples collected at each point).

absorbance at 254 nm (SUVA254) ( Fig. 3.a). This parameter is considered a useful proxy for DOM aromatic content and molecular weight in environmental matrices [74,75], it correlates positively and linearly with the aromaticity of CDOM [31,42].

The SUVA254 values obtained here are typical of surface waters [75, 76], mainly distributed between 1 and 6 $L.mg^{-1}.m^{-1}$. The upstream water source P1 showed a broad distribution of SUVAs in the range 2–4 $L.mg^{-1}.m^{-1}$, and so this interstitial water may be dominated by terrigenous OM [47]. Similar values were reported for a pristine African tropical watercourse in the Congo [76]. The relatively low SUVA254 values observed for sampling points P2 and P3 lead to the assumption that the released oil mill wastewaters are rich in protein-like or fresh OM; a fresh material contains significantly fewer aromatic rings than humic substances. As expected from the DOC measurements, the SUVA254 values were substantially higher at point P4, as its waters are a combination of low-flow waters from P2 and P3 and high-flow waters from P1. In contrast, SUVA254 values were higher for the WWTP effluents (sampling point P6) than the influents (sampling point P5), which indicates that the natural lagoon process preferentially removed non-aromatic carbon components. Other studies have reported increased SUVA values in treated sewage [77]. The downstream sampling point P7 showed relatively higher SUVA values, which may be due to absorption at 254 nm from iron, colloids, or other constituents, as point P7 is the confluence of all the water streams [21].

Across all the river sampling points P1 to P7, the calculated absorbance E2/E3 and E2/E4 ratios showed similar overall patterns (Fig. 3.b, Fig. 3.c). Consistently with the variation in SUVA254 along the river, the upstream source P1 dominated by terrestrial OM presented the lowest E2/E3 value, nearing 2.5, whereas all other sampling points except P5 presented values ranging between 3.5 and 3.9, which are indicative of mixed OM with different degrees of humification, the highest of which was found for P1 water. The WWTP influent point P5 showed a unique pattern of an E2/E3 absorbance ratio very close to 5.5, which is unsurprising as raw wastewaters are rich in protein-like material. As expected, the E2/E4 absorbance ratio showed similar variation through all sampling points with values lower than 8.5, while the influent wastewaters at P5 gave a value of around 11. These changes suggest that from the upstream source P1 down to the other sites, DOM shifts from a terrestrial humic-rich OM toward mixtures with smaller and less aromatic compounds [78].

The $S_{275–295}$ spectral slope of the natural logarithm of absorbance as well as the slope ratio (SR) between 275–295 nm and 350–400 nm obtained for the upstream water source P1 were lower than 0.014 $nm^{-1}$ and 1, respectively (Fig. 3.d, Fig. 3.e). This is consistent with the SUVA and E2/3 parameters obtained above, and highlights a terrestrial humic-rich water. All the other sampling points gave globally higher slopes and higher ratios, indicating that as we move downstream, the DOM shift towards less humic fractions and lower-molecular-weight material due

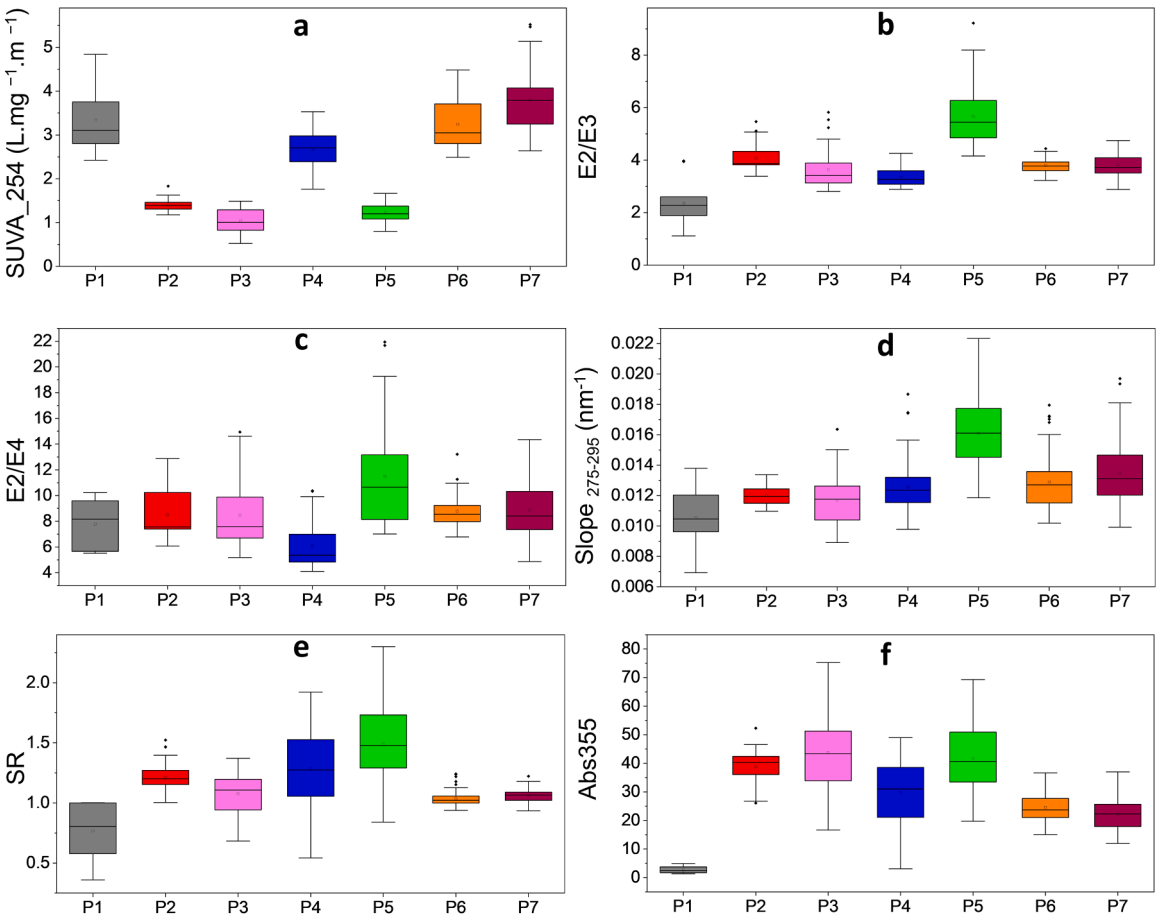


**Fig. 3.** UV-Vis absorption indicators of the water samples collected along the Ben-Kazza River. a: SUVA254, b: E2/E3 (Abs250/Abs365), c: E2/E4 (Abs254/Abs436), d: Slope (275_295 nm-1), e: slope ratio (S275_295/S350_400), f: Absorption coefficient (Abs355 nm).

to decreasing aromaticity. This behavior is obviously due to the discharges of the oil mill and the WWTP effluents into the river, enhanced by sunlight irradiation [78].

However, when comparing their spectral slopes and ratios, the upstream WWTP influents point (P5) and the downstream effluent point (P6) stood out from the rest. The decrease in both parameters in the effluent compared to influent waters cannot be attributed to an enhancement of aromatic fractions in the effluent DOM, since as we saw with the SUVA values, the natural lagoon process preferentially removed non-aromatic carbon components. Consequently, it is more likely that the observed decrease is induced by exposure to direct sunlight at decantation during the natural lagoon treatment. A similar pattern of SR ratio behavior has been reported by other authors [52]. All these parameters may complete and enrich the global water quality ones based on other analyses such as COD and BOD5 measurements.

### 3.3. Excitation-emission/PARAFAC exploration of DOM

The optically-active DOM fractions are protein-like and humic-like, which are characterized by emission at wavelengths lower than 380 nm and higher than 380 nm, respectively [9]. The relative distribution of these fluorescence components generally helps to distinguish DOM sources between forested streams, agricultural streams, groundwaters, marine waters, and domestic or urban wastewaters, as well as oil mill wastewater discharges [10,59,79].

Ben-Kazza River, originally supplied by the groundwater source feeding the sampling point P1, is expected to have an almost constant content and quality of fluorescent OM, and so any additional in-feeding surface water or wastewater would bring about changes in the river's DOM fluorescence signatures [80]. To explore these changes, we investigated samples of river water using EEM/PARAFAC in order to i) examine the distribution of different DOM fluorophores across the river, and ii) estimate DOM removal efficiency within the WWTP discharging into the river at point P6. For that purpose, we determined the DOM fluorophores and fluorescence indices and correlated them with the absorption indicators considered above. All 495 samples collected were explored by excitation–emission measurements in tandem with PARAFAC chemometrics.

Fig. 4 charts the patterns of experimental EEMs corresponding to each sampling point, from P1 to P7. The spectral loadings corresponding to the excitation–emission maxima values of each PARAFAC component are shown in Fig. S4 and Fig. S5, while the λex/λem characteristics of the PARAFAC components are given in Table 3. Fig. S6 plots the fluorescence indices HIX and BIX, calculated as described in Table S1, and averaged over all samples.

#### 3.3.1. Upstream source P1

The experimental excitation–emission landscape corresponding to water source P1 (Fig. 4. P1) shows three main fluorescence regions at 230–300 nm/330–400 nm, 230–280 nm/400–500 nm, and 300–370 nm/400–500 nm excitation/emission, often referred to as humic material and commonly observed in groundwaters [81]. An additional very-low-intensity and red-edge fluorescence region is also observed at 230–450 nm/500–600 nm. PARAFAC analysis resulted in three components (C1, C2, and C3; Fig. 5. P1). Component C1_P1 (275–330 nm/380 nm) and component C2_P1 (265–355 nm/450 nm), which are respectively associated to peak M and humic-like materials, are widely observed in natural waters [59]. Peak M indicates the

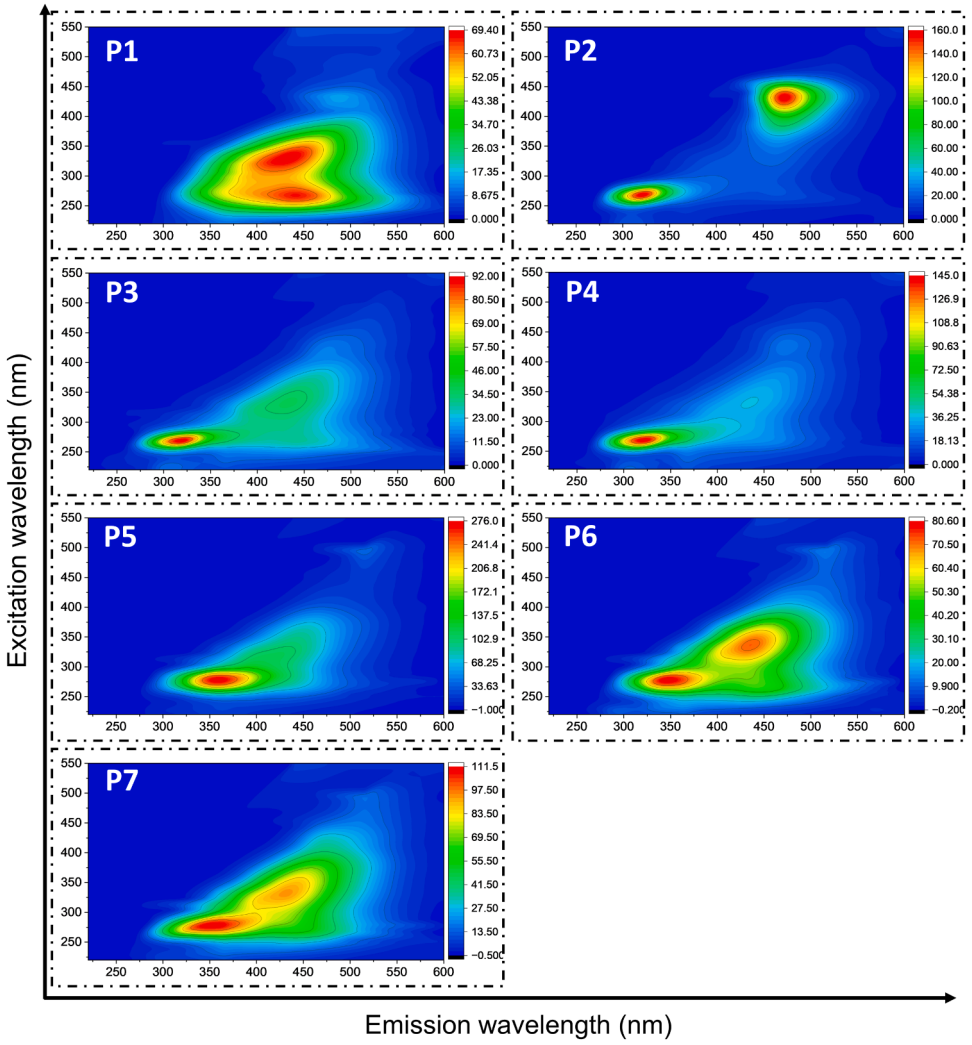


**Fig. 4.** Examples of experimental fluorescence excitation-emission matrices (EEMs) measured on the collected water samples (P1 to P7).

presence of organic material from recent biological activity (soluble microbial humic-like material) [82,83]; components similar to component C1 have been reported for groundwaters [84]. The third component C3_P1 (260–420 nm/525 nm), with two excitation peaks, appears similar to component C2 identified by Ishii et al. (2012) in natural systems and associated to UVC humic-like and UVA humic-like material [58]. The secondary peak at 420 nm/525 nm indicates that this component C3_P1 consists of large-molecular-weight hydrophobic compounds [85] positively associated with apparent molecular weight [86] and susceptible to UVA-induced photodegradation [87]. It may derive from terrestrial organic matter rich in humic content [88].

The absence of any protein-like fluorescence signal indicates the absence any kind of microbial/biological anthropogenics; indeed, the water source is far from any source of contamination. The calculated fluorescence indices FI, BIX and HIX are around 1.55, 0.65 and 4.3, respectively. FI is indicative of a DOM combining terrestrial and microbial sources likely related to the soluble microbial humic-like material, as revealed by PARAFAC component C1_P1 (or peak M). The value of the BIX index (0.6–0.7), which is well below 1, can be associated with a low biological production of autochthonous-origin OM [10,89]. The HIX index, very close to 4, is indicative of a weak humic character and/or the presence of recent autochthonous organic material. This is consistent with the occurrence of peak M reflective of the presence of an organic material from recent biological activity.

### 3.3.2. *Downstream points P2, P3 and P4*

**Point P2.** The experimental EEM together with the PARAFAC components obtained for waters sampled at point P2 are given in Fig. 4. P2. The EEM revealed two main fluorescence regions, at 250–290 nm/ 280–380 nm and at 350–460 nm/ 440–540 nm, very different from those obtained for the sampling point P1. PARAFC analysis led to five components (Fig. 5. P2): the first two components C1_P2 and C2_P2, both located at emission wavelengths lower than 380 nm, present very different emission and excitation features from those typically reported for protein-like fluorescence [59]. Component C1_P2 at 270 nm/320 nm could correspond to a polar phenolic-like compound [90,91], whereas component C2_P2 at 270 nm/290 nm may be related to an anthropogenic cresol-like fluorophore, likely a pesticide residue [9]. Component C3_P2 at 430 nm/470 nm, located above 380 nm and which does not correspond to any humic-like signal reported in waters [92,93], could be associated with oxidation products of vitamin E originating from olive oil waste [94]. Nevertheless, it worth noting that both tocopherols and polyphenols absorb and emit in the same ranges [95,96]. Component C4_P2 at 230–280 nm/380 nm, emitting in the UV region, appeared somewhat similar to peak M often observed in natural waters, and could be related to organic fluorophores emerging from recent biological activity [97]. Component C5_P2 observed at 260–360 nm/450 nm is almost certainly due to the humic-like DOM fraction in the water driving the oil mill waste, and corresponds to component C2_P1 observed in the waters sampled on the upstream source P1. Table 4 reports comparative

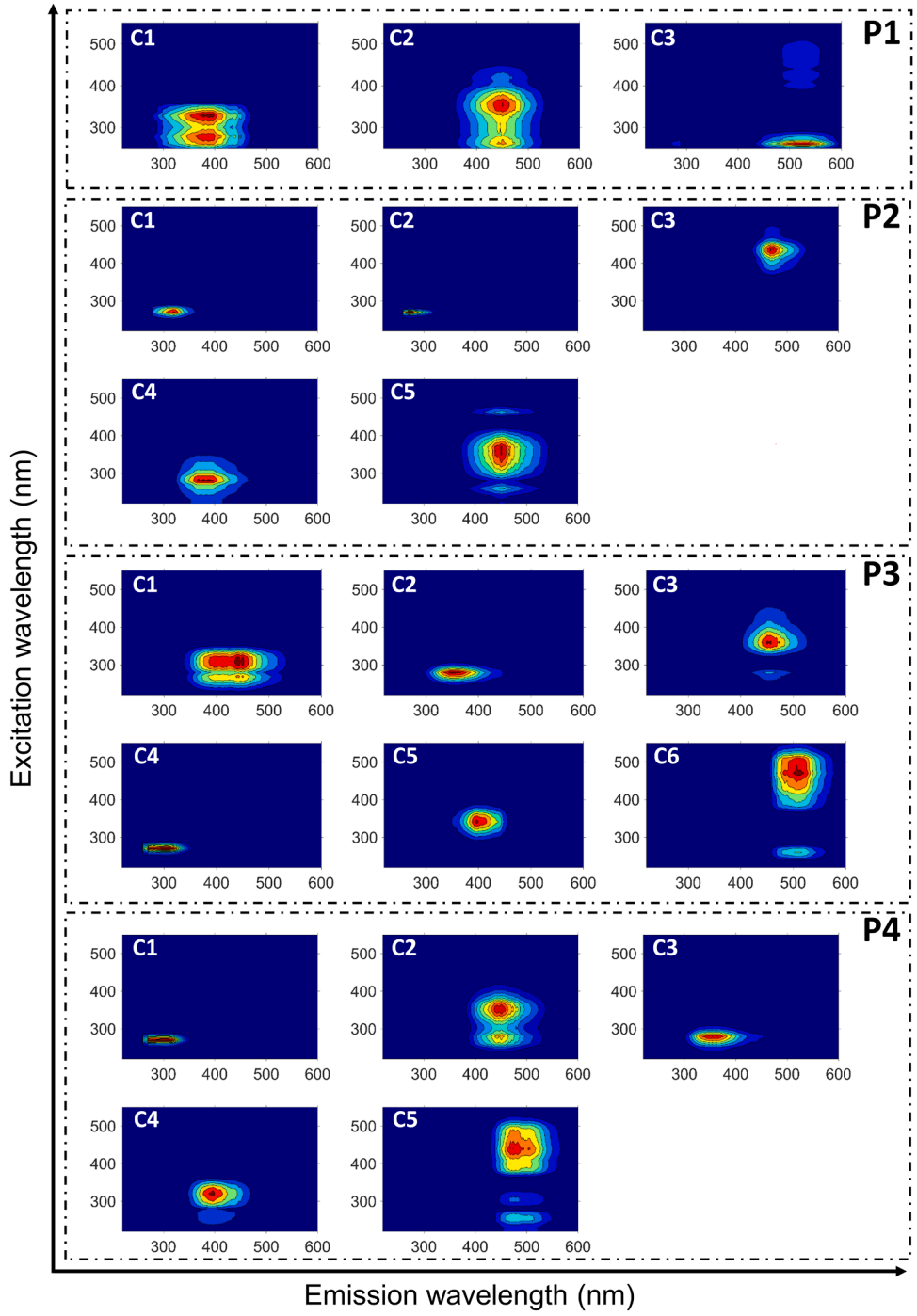


**Fig. 5.** PARAFAC components corresponding to sampling sites P1, P2, P3 and P4.

**Table 3**
PARAFAC components based on excitation–emission wavelengths. (λex ± 5 nm/λem ± 10 nm; nd: not detected).

| Sampling points | | | | | | | |
|---|---|---|---|---|---|---|---|
| Component | P1 | P2 | P3 | P4 | P5 | P6 | P7 |
| C1 | 275–330/380 | 270/320 | 270–310/440 | 270/300 | 280/355 | 260–315/400 | 275/355 |
| C2 | 265–355/450 | 270/290 | 280/350 | 280–350/450 | 270–350/440 | 270–350/445 | 275–355/450 |
| C3 | 260/420/525 | 435/470 | 280_360/455 | 275/355 | 305/400 | 285/350 | 320/400 |
| C4 | nd | 230–280/380 | 270/295 | 260–325/400 | 270–380/465 | 270–380/470 | 270–390/470 |
| C5 | nd | 260–360/450 | 340/400 | 260–440/475 | 270/300 (375) | 260/(350) 450 | 270/300 |
| C6 | nd | nd | 260–470/515 | nd | 260–495/520 | 260–340–495/520 | 265/(380) 445 |
| C7 | nd | nd | nd | nd | nd | nd | 280–495/520 |

analysis and similarity between the PARAFAC components through the seven sampling points.

**Point P3.** The excitation–emission landscape collected on the oil mill wastewaters sampled at site P3 (Fig. 4. P3) is clearly different from the previous landscape corresponding to site P2. It exhibits two large and overlapped fluorescence regions, with two main peaks at 250–290 nm/270–350 nm and at 250–400 nm/390–500 nm, and a lower-intensity red-edge fluorescence around 450 nm/500 nm. PARAFAC analysis resulted in six components (Fig. 5. P3), C1 to C6. Component C1_P3 (270–310 nm/440 nm) with two excitation sub-regions could be related to humic material probably interacting with by-products of the vegetable oil refining process. Component C2_P3 (280 nm/350 nm) presents excitation and emission features of protein-like components, but polar phenolic-like compounds also present similar absorption and emission positions [98]. Component C3_P3 (280–360 nm/455) is quite similar to components C5_P2 and C2_P1, both of which were attributed to humic-like fluorophores in the water body, whereas component C4_P3 (270 nm/295 nm) appears analogous to component C1_P2 associated to polar phenolic-like fluorophores. Component C5_P3 (340 nm/400 nm) presents absorption and emission spectral ranges, maxima and shapes comparable to those previously found for some carbamates used as fungicides such as the commercial product (Ridomil Gold MZ 68) [99]; this residue could be entrapped in humic fractions of the water OM. Component C6_P3 (260–470 nm/515 nm) is likely a residual riboflavin-like fluorophore in the oil mill wastewater [100–102]. Riboflavins (vitamin B group) are a family of yellow-colored compounds with the basic structure of 7,8-dimethyl-10-alkylisoalloxazine. They are characterized by absorption in the ultraviolet and visible regions and an intense yellow-green fluorescence, and they are stable when heated and leach into hot water, but degraded by light [103].

**Point P4.** The experimental excitation–emission landscape collected on the waters sampled at the downstream point P4 (Fig. 4. P4) is very similar to the landscape corresponding to point P3, although it also gathers waters from point P2 (Table 4). Four overlapping fluorescence regions can be distinguished, at 250–300 nm/270–350 nm, 250–350 nm/370–430 nm, 250–370 nm/440–470 nm, and 350–480 nm/450–520 nm, while five PARAFAC components (C1 to C5) were obtained (Fig. 5. P4). Components C1_P4 (270 nm/300 nm) and C3_P4 (275 nm/355 nm) are the same as the above components C4_P3 and C2_P3, and show very similar loadings. Component C2_P4 (280 nm/350 nm) is the same as component C2_P1 and C5_P2 attributed to humic-like material in the natural groundwater DOM. Component C4_P4 (260–325 nm/400 nm) appears fairly similar to the humic-like component C1_P1. However, component C5_P4 (260–440 nm/475 nm) exhibits very particular features and was not observed in any of the sites P1, P2 nor P3. This component could be associated to a yellow dye-like fluorophore, as its absorption maximum was around 430 nm. The existence of more than one excitation peak is most probably related to electron transitions from the ground state to different higher-energy excited states. However, because of the lack of data on EEMs relative to oil mill wastewaters in the literature, it is difficult to confidently identify all the PARAFAC components obtained in the present case. Oil mill wastewaters are by-products including various compounds such as lipids, phenols, polyphenols, organic and inorganic constituents in addition to nutrients, with high levels of chemical oxygen demand [104]. This wide variety of compounds is also revealed by fluorescence of olive oil compost [105].

The characterization of DOM from sites P2, P3 and P4 was further investigated by the determination of the BIX and HIX indices (Fig. S6) to give more insight in the variation of water DOM through these sampling points. We did not use the fluorescence index (FI) here, as previous reports conclude that it is not suitable as a parameter for waters whose organic material comes from a diversity of sources and contains significant amounts of non-humic substances [10,106], as is the case for water containing oil-mill waste effluents. The BIX values obtained for waters sampled at points P2, P3 and P4 are distributed in the ranges 0.87–0.93, 0.80–0.88 and 0.80–0.83, respectively, while the HIX values were distributed around 0.20–0.25, 1.20–1.30 and 0.4 –1.75, respectively. The fact that all these BIX indicators are in the range 0.80–1.0 indicates freshly-produced organic materials in all three sampling points. The HIX values, all very low, also indicate freshly-produced organic material. Consequently, both fluorescence parameters are consistent with the nature of the sources feeding the sampling points, which are particularly rich in oil-mill wastewater. Similar values have been reported for municipal wastewater in Eastern China [107]. However, the relatively low HIX values at point P2 could also indicate stronger microbial activity [24], given that point P2 is a secondary water source that is likely to be contaminated by hidden leakage form the oil mill wastes. The HIX values for point P4, scattered between 0.40 and 1.75, reflect the fact that this point gathers waters from both P2 and P3 in addition to the flow of water from P1. Furthermore, all points P2, P3 and P4 show lower HIX values and higher BIX values than the upstream point P1 which is fed by older organic matter with a higher degree of humification. This is also consistent with the variation in E2/E3 absorbance ratio discussed above.

### *3.3.3. WWTP influents and effluents: DOM characterizing and assessment of treatment performance*

In wastewaters, a low OM content is considered as indicator of good water quality, and the efficiency of water treatment is commonly assessed on the basis of OM fractions removal [5]. Hence, before considering the downstream point P7, which is the outlet of all upstream watercourses, it is important to consider the sampling points P5 and P6 receiving the WWTP influent and effluent waters. The goal is to assess the efficiency of this WWTP that uses natural lagoon across successive ponds for a period varying between 13 and 17 days.

#### *3.3.3.1. Characterization of DOM in the influent and effluent waters.*

Fig. 4 reports the patterns of the experimental EEMs corresponding to influent (P5) and effluent (P6) waters. These water fluorescence landscapes exhibited similar shapes characteristic of wastewaters [10], with three overlapping fluorescence regions at 240–300 nm/300–400 nm, 240–300 nm/400–500 nm, and 300–430 nm/400–500 nm, with an additional low-intensity red-edge fluorescence. The three regions are those commonly known as peak T1, peak A/M, and peak C, respectively associated with protein-like (tryptophan) material, fluvic-like/soluble microbial humic-like material, and humic-like material [108]. As expected, the main difference between the influent and effluent landscapes concerned the variation in relative intensity of the first fluorescence region (peak T1) versus the third one (peak C), as the fluorescence intensities of these two well-resolved regions were not equally reduced between influents and effluents. The decrease in intensity between raw and treated waters was about 75% for peak T1 but only 22% for peak C.

PARAFAC analysis led to six components (C1 to C6) for both sites. Based on the wavelength ranges in emission and excitation (Fig. 6), component C1_P5 (280 nm/355 nm) was identified as a protein-like fluorescence most likely related to tryptophan amino acid [9,59]. This fluorescence region has been also associated with living and dead cellular materials and their exudates in fecally-contaminated wastewater. It indicates microbial activity [109] and material derived from anthropogenic activities [110]. This component also shared spectral similarities with many pharmaceutical products, such as diclofenac, lamotrigine, naproxen, propranolol HCL, salbutamol, sulfamethoxazole, trimethoprim, and others. Consequently we cannot rule out that this fluorophore could also contain pharmaceutical-like protein substances [56], as pharmaceutical compounds are regularly found in WWTP effluents [111]. Component C2_P5 (270–350 nm/440 nm) showed primary and secondary excitation peaks that very likely point to humic-like with fulvic-like materials commonly related to peaks C and A [10]. A similar component was identified in other studies [58] and labelled component E by Murphy et al. [59]. Another similar component, designated by peak W, has also been detected in several studies on the

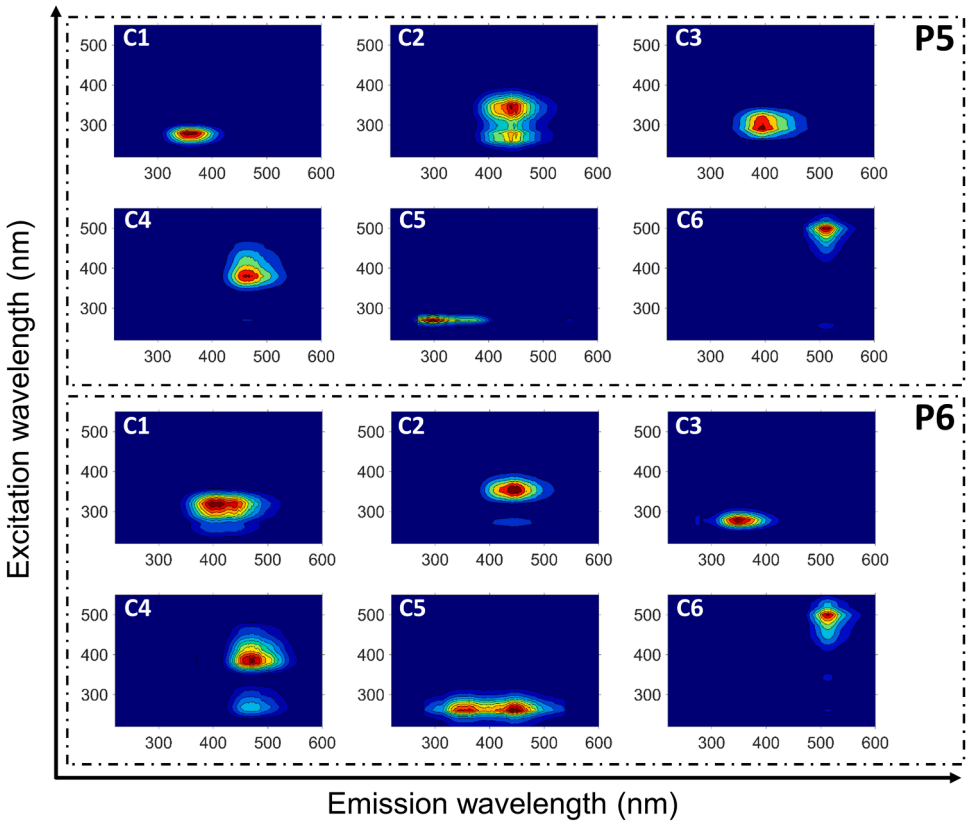


**Fig. 6.** PARAFAC components corresponding to sampling points P5 and P6.

fluorescence of detergents, in particular 4,4′-bis(2-sulfostyryl)disodium biphenyl (DSBP) and diaminostilbene [112,113]. These substances, which are fluorescent bleaching agents, represent a form of anthropogenic DOM that is widely ubiquitous in polluted rivers, and they are known to be very poorly degradable [114]. Component C3_P5 (305 nm/400 nm) could be approximated as peak M related to soluble microbial humic-like material and indicating the presence of organic compounds from recent biological activity [10]. However, a number of pesticides show similar fluorescence patterns, such as diflufenican, fludioxonil, norflurazon, pirimicarb and others [56], which could thus link this fluorophore to pesticide-like humic substances [115]. Component C4_P5 (270–380 nm/465 nm) exhibits a high-intensity excitation peak at 380 nm along with a very-low-intensity secondary peak at 270 nm. It appears to originate from a mixture of fluorophores that emit over the same wavelength range, mainly resembling Coble's peak C but also peak A [116]. Peak A was attributed to high-molecular-weight humic-like substances while peak C indicates more aromatic humic matter than peak A [117]. Other authors reported a similar component in WWTP influents and effluents and associated it with a high-molecular-weight hydrophobic humic-like component thought to be exported from terrestrial sources [24,118]. Component C4_P5 could be attributed to humic-like compounds found across areas rich in nutrients and affected by sewage water [97].

Component C5_P5 (270 nm/300 nm, 380 nm) shows spectral characteristics very different from those commonly known for DOM fluorophores, and is obviously related to an anthropogenic fluorophore. Note that the commercial fungicide Orsalis 5% SC is widely used in Morocco and exhibits similar spectral features [99]. A possible explanation for the observed bimodal nature of the emission spectrum could be either intra-molecular formation of charge-transfer complexes in the excited state or excimer formation [55], or the existence of different conformations in the excited sate [119]. Nevertheless, phenanthrene, which fluoresces in the same region, cannot be ruled out [120]. Phenanthrene is a polycyclic aromatic hydrocarbon (PAH) generally formed during incomplete anthropogenic combustion of OM; in rural zones such as Aïn Taoujdate, wood is still widely used as a fuel source. Component C6-P5 (260–340–495 nm/520 nm) is a really intriguing fluorophore absorbing and emitting at the red edge of the spectrum, far from any other DOM signals. This component could originate from any anthropogenic colored-like free fluorophore with a relatively low contribution in the entire fluorescence response of the WWTP influent waters. Fluorescein and its derivatives, widely used as dyes, have similar fluorescence characteristics [121,122].

Considering all the effluent waters discharged by the WWTP at point P6, five of the six components highlighted by PARAFAC analysis (C1, C2, C3, C4 and C6) respectively matched to the components (C3, C2, C1, C4 and C6) found in the influent waters from point P5 (Table 4). Component C5_P5 was not recovered in P6 effluent waters, but a new fluorophore C5_P6 emerged in these P6 effluents. The new emerging component C5_P6 (260 nm/(350 nm), 450 nm) exhibits two well-resolved fluorescence peaks with relative intensities that are independent of excitation wavelength, and shows emission loading with a vibrational shape very similar to what is commonly observed for PAHs. Furthermore, the wavelength ranges of the excitation–emission loadings seem to indicate that the PAH could be likely a congener of fluoranthene that absorbs in the ranges 265–300 nm (S0_S2) and 300–390 nm (S0_S1), and emits in the range 400–600 nm with an emission maximum at 450 nm [123]. Incomplete burning of wood, coal, and organic matter is a major source of this pollutant, which is also produced by many industrial processes [124]. Furthermore, in the influent waters sampled at point P5, the non-appearance of component C5_P6 may be explained by a fluorescence quenching effect induced by the high content of anthropogenic OM. It has been experimentally demonstrated that a high OM content induces fluorescence quenching of many organic pollutants in wastewaters, whereas OM abatement enhances their fluorescence [125]. On another side, the component C5_P6 may not be seen as a soluble

microbial product (SMP), often identified on biologically treated effluent wastewater, as SMP usually show fluorescence landscapes different from that revealed by this component [126]. Nevertheless, it is not excluded that during the long lagoon process, the fluorophore C5_P5 could be transformed into the fluorophore C5_P6 (PAH). Also, it is worth noting that exchanges between dissolved organic matter (DOM) and particulate organic matter (POM) play a critical role in the mobility and bioavailability of pollutants in surface waters [127].

*3.3.3.2. Evaluation of the WWTP performances.* To assess the efficiency of the wastewater treatment and characterize DOM removal by lagoon treatment, we tracked the extracted PARAFAC components via their maximum fluorescence intensities (Fmax) across the wastewater treatment (Fig. 7). The Fmax values are considered to be proportional to the relative concentrations of the different components [128]. Over the course of the lagoon treatment, and consistently with the measured DOC as well as the measured fluorescence intensities, Fmax decreased on all components, leading to a ΣFmax decrease of more than 55%. This was expected, as the measured DOC values decreased from influents to effluents (Table 2). Furthermore, considering the effect of lagoon treatment on the relative contributions of protein-like material and humic-like material in the overall fluorescence signal, between raw water and treated water, the relative contribution of the protein-like component decreased from 35% (C1_P5) to 25% (C3_P6) while the relative contributions of humic-like components increased from 18% (C2_P5) to 27% (C2_P6), from 17% (C3_P5) to 25% (C1_P6), and from 8% (C4_P5) to 10.5% (C4_P6). These patterns are perfectly being consistent with the UV-Vis absorption indicators that showed an increase in SUVA254 values in parallel with a decrease in E2/E3 and E2/E4 absorbance ratios, all related to an increase of aromaticity in the water DOM. This aromaticity behavior is also highlighted by the increase in HIX values in parallel with a clear decrease in BIX from influent to effluent waters (Fig. S6). The increase in HIX after the long settling periods in the successive lagoon ponds could imply either a transformation of small protein molecules into humic-like substances [129] or a more efficient removal of non-aromatic OM than aromatic material. The lagoon process also reduced the relative contribution of anthropogenic organic pollutants in the entire fluorescence signal from 22.3% (C5_P5 and C6_P6) to 12.3% (C5_P6 and C6_P6).

Other WWTPs based on lagoon process, such as that of Aïn Chiffa in Sefrou city, have been assessed on the basis of other parameters, such as BOD5, COD and suspended matter [130]. Here, we find that fluorescence intensities with HIX values are rapid fluorescence indicators suitable for real-time monitoring of the efficiency of wastewater treatment by natural lagoon. Nevertheless, in addition to absorption indicators, other readily accessible parameters such as conductivity, turbidity, suspended solids, pH and chroma [131] may also be considered to usefully refine the assessment of treatment efficiency. In the present case, the lagoon treatment has decreased the conductivity by about 15%.

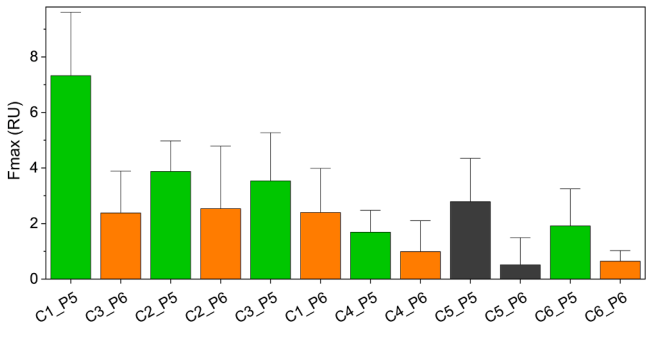


**Fig. 7.** Variation of fluorescence intensity Fmax values (in Raman units) from influents to effluents. (Gray column represents non-similar components).

*3.3.4. Fate of DOM downstream*

After describing the water DOM at the original groundwater source and across all sampling sites, we looked at water samples from the confluence point P7, which also includes possible runoff from neighboring agricultural fields. The fluorescence landscape of waters from this point P7 (Fig. 4. P7) is characteristic of contaminated surface waters [10], exhibiting a protein-like/microbial-like fluorescence area (250–300 nm/330–400 nm) as the higher intensity region, a lower-intensity humic-like region at 280–375 nm/380–500 nm, a fulvic-like region at 240–300 nm/400–500 nm, and a red-edge low intensity fluorescence region. PARAFAC analysis led to 7 components (C1_P7 to C7_P7; Fig. 8) with the following excitation–emission characteristics: Component C1_P7 (275 nm/355 nm), component C2_P7 (275–355 nm/450 nm), component C3_P7 (320 nm/400 nm), component C4 (270–390 nm/470 nm), component C5_P7 (270 nm/300 nm), component C6_P7 (265 nm/(380 nm), 445 nm) and component C7_P7 (280–495 nm/520 nm) (Table 3). As highlighted by the loading shapes, all these components match those already identified in the upstream sampling points.

Table 4 shows the similarities between each point for mTCC > 74. Strikingly, neither component C3_P1 (UVC humic-like with UVA humic-like material) nor component C5_P4 (a yellow dye-like fluorophore) appeared in P7 samples. This may be explained by solar radiation-induced photodegradation, as these large-molecular-weight fluorophores may be photodegraded before the other anthropogenic organic pollutants. In terms of the relative contribution of each category of fluorophores to the entire fluorescence signal (Fig. S7), the overall humic-like material (C2, C3 and C4 at point P7) contributes about 50%, protein-like material (C1_P7) contributes 31%, while free anthropogenic organic pollutants (C5_P7, C6_P7 and C7_P7) contribute the remaining 19%. For the upstream water source P1, which is far from any source of organic pollution, humic-like material contributed 100%. This observed variation in fluorescent DOM between the upstream groundwater source P1 and the downstream confluence point P7 was further highlighted by HIX and BIX fluorescence indicators. The humification index HIX showed a drastic decrease, while the biological index BIX showed a strong increase, revealing a loss of humification accompanied by the production of recent organic material from biological/microbial activity. Very likely solar radiation is also contributing to the observed shift of fluorescent DOM towards low molecular and less aromatic material [87].

*3.3.5. Spatiotemporal variability of DOM in a river*

To get a better understanding of the spatial shift in DOM between the upstream source P1 and the far downstream confluence point P7, and track the time-course change in DOM between the two sampling-campaign periods, we ran a multivariate statistical PCA on 17 absorbance and fluorescence parameters and a set of 110 water samples collected at sites P1 and P7. The intermediate points have not been considered as they all have a direct impact on the downstream P7 zone. Principal components (PCs) represent maximum variance in the set of samples and therefore describe the spectral factors that changed most significantly between samples. Here, the parameters considered in the analysis were $A_{355}$, E2/E3, E2/E4, $S_{275–295}$, $S_R$, BIX and HIX, along with relative abundance scores (% Fmax) corresponding to the 10 components of the two sites P1 and P7.

Analysis of these parameters resulted in two principal components (PC1 and PC2) that accounted for 88.5% of the total variance in the dataset (Fig. 9). PC1 explaining 73% of the variance appeared to be principally related to the size of the fluorescent DOM fractions; it is positively correlated to BIX and negatively correlated to HIX. The second component PC2 explaining 15.5% of the variance appeared to concern the type of pollutant in the water, as reflected by the PARAFAC components. PC2 is positively correlated to component C6_P7 and negatively correlated to component C5_P7.

Fig. 9.a and 9.b show respectively the loading plot of all variables

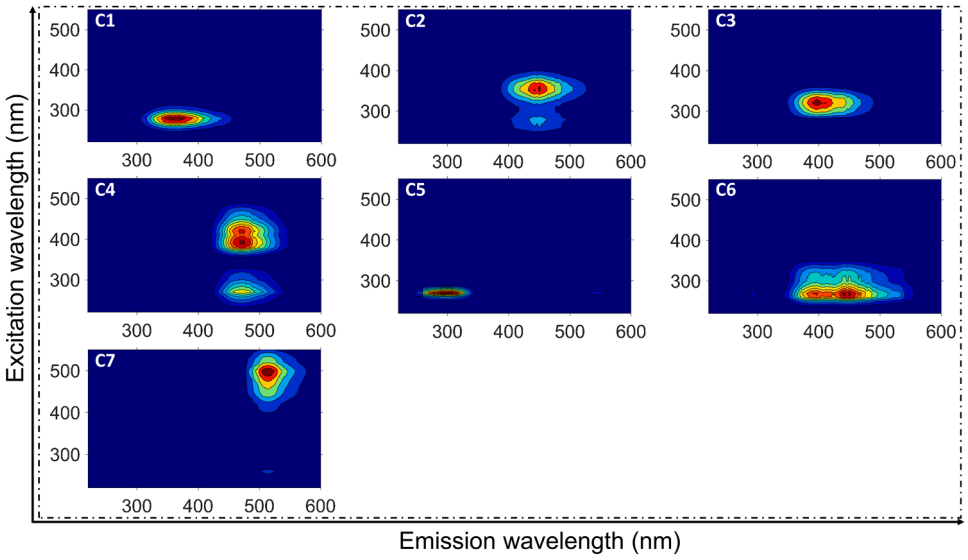


**Fig. 8.** PARAFAC components corresponding to sampling point P7.

**Table 4**
Similarity factors between the PARAFAC components.

| | | | | | | |
|---|---|---|---|---|---|---|
| mTCC (P1/P2) | | | C2_P1/C5_P2 0.80 | | | |
| mTCC (P1/P4) | | | C2_P1/C2_P4 0.84 | | | |
| mTCC (P2/P3) | | C1_P2/C4_P3 0.84 | | | C2_P2/C4_P3 0.78 | |
| mTCC (P2/P4) | C1_P2/C1_P4 0.82 | C2_P2/C1_P4 0.80 | C3_P2/C5_P4 0.81 | C4_P2/C3_P4 0.78 | C5_P2/C2_P4 0.92 | |
| mTCC (P3/P4) | | C2_P3/C3_P4 0.97 | | | C4_P3/C1_P4 0.99 | |
| mTCC (P5/P6) | C1_P5/C3_P6 0.97 | C2_P5/C2_P6 0.80 | C3_P5/C1_P6 0.90 | C4_P5/C4_P6 0.94 | C6_P5/C6_P6 0.97 | |
| mTCC (P2/P7) | | C1_P2/C5_P7 0.80 | | | C2_P2/C5_P7 0.81 | |
| mTCC (P3/P7) | | C2_P3/C1_P7 0.95 | | | C4_P3/C5_P7 0.99 | |
| mTCC (P6/P7) | C1_P6/C3_P7 0.95 | C2_P6/C2_P7 0.95 | C3_P6/C1_P7 0.95 | C4_P6/C4_P7 0.96 | C5_P6/C6_P7 0.80 | C6_P6/C7_P7 0.98 |

and the score plot of all samples onto the PC1 × PC2 plane. These diagrams reveal clear differences in DOM composition between the two sampling points and between the two sampling campaigns. The spatial shift in DOM appears to be governed essentially by the size of the chromophores: Waters from the upstream source P1 correlate positively with HIX and PARAFAC components associated with humic-like material. In contrast, waters from the downstream confluence point P7 correlate positively with BIX, reflecting biological/microbial activity at the sampling point, and with PARAFAC components associated with either protein-like or pollutant-like materials. Additionally, the absorbance at 355 nm indicates the degradation of water quality. Time-course analysis did not detect any change in DOM at the upstream source P1, while DOM clearly changed at the downstream confluence point P7. The sample distribution on the PC1 ×PC2 plane clearly shows two sets of samples according to the sampling campaign. Samples from the first campaign (March and April 2022) correlated positively with PARAFAC

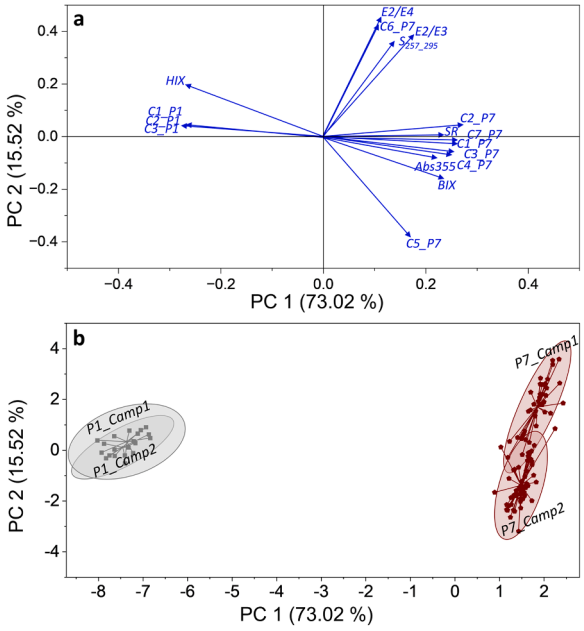


**Fig. 9.** Sampling points P1 and P7. Principal component analysis: a) loading plots of all variables and b) score plots of all samples on the PC1 × PC2 plane. Ellipses represent identifiable sample groups.

component C6_P7, whereas samples from the second campaign (May and June 2022) correlated with PARAFAC component C5_P7. PARAFAC component C6_P7 has been associated with a PAH-like fluorophores and PARAFAC component C5_P7 has been associated with polar phenolic-like fluorophores. This is not surprising, as the downstream waters at site P7 were highly impacted by wastes discharged from upstream intermediate sites, i.e. P6 and P3. These wastes change according to the activities of the neighboring WWTP (P6) and the oil mill facility (P3).

Although this statistical analysis did not show any strong positive correlation with any of the initial spectral factors, the spatial shift in DOM appears governed by fluorophore size and biological/microbial activity of the OM, while temporal change appears more related to the kind of the organic pollution reaching the downstream waters.

## 4. Conclusion

This study investigated the combination of UV-Vis. absorption and of EEM-fluorescence supported by PARAFAC and PCA chemometrics to track fluorescent DOM in surface waters in Morocco, specifically in the Ben-Kazza River in the Fez–Meknes region. We addressed two main issues: i) the spatial and temporal changes in DOM across the river subject to different sources of effluent discharges, and ii) the efficiency of the lagoon treatment provided by the Aïn-Taoujdate WWTP. Our approach highlighted a surface water that was typical of river water impacted by wastewater inputs, with significant amounts of protein-like material in addition to anthropogenic organic pollutants likely related to pesticides, dyes, PAHs and pharmaceuticals. Moreover, in addition to the spatial changes in the DOM of the river due to the variability of the in-feeding sources, we also highlighted temporal changes in DOM due to the temporal variability in anthropogenic activities around the river area.

The assessment of the efficiency of the lagoon treatment in the adjacent wastewater treatment plant showed that it removed about 55% of the DOM and was more efficient on fresh organic material. Humic material and anthropogenic organic pollutants were more refractory.

Overall, this investigation showed that the combination of UV-Vis absorption and excitation-emission fluorescence is suitable as a low-cost approach to: i) monitor real-time changes in DOM along the watercourse, and ii) assess lagoon WWTP treatment. These analytical methods, are relevant, cost-effective, and do not require specific high-level skills. They are ideally suited for rural communities, making them well positioned to meet the growing need for efficient monitoring of harmful environmental contaminants in surface waters.

This ongoing investigation is now focusing on the long-term impact of irrigation by the partially-treated WWTP effluents on the irrigated agricultural soils.

## Environmental implication

This study focused on identifying the sources and distributions of anthropogenic contaminants from wastewater and partially treated effluents discharged into the Ben-Kazza River as a surface water. It is based on crossing UV-Vis absorption, EEM fluorescence and chemometrics. The high levels of DOM detected at the discharge points correlate with the occurrence of various pollutants such as phenols, pesticides and pharmaceuticals. These contaminants pose a risk to livestock drinking from the river and to agricultural soils irrigated by these surface waters. The investigation represents a relevant and cost-efficient approach to monitoring harmful pollutants in surface waters.

## CRediT authorship contribution statement

**Christelle MARGOUM**: Writing – review & editing, Validation, Supervision, Project administration, Methodology, Funding acquisition. **Abdelmajid EL BAKKALI**: Visualization. **Saadia AIT LYAZIDI**: Writing – review & editing, Validation, Supervision, Project administration, Funding acquisition. **Omar TAOUSSI**: Visualization, Investigation. **Hassan BA-HADDOU**: Writing – original draft, Visualization, Software, Methodology, Investigation, Formal analysis, Data curation, Conceptualization. **Mustapha HADDAD**: Resources, Funding acquisition. **Matthieu MASSON**: Visualization, Validation, Methodology, Conceptualization. **Marina COQUERY**: Writing – review & editing, Validation, Supervision.

## Declaration of Competing Interest

The authors declare that they have no known competing financial interests or personal relationships that could have appeared to influence the work reported in this paper.

## Data availability

Data will be made available on request. The database associated with this article can be found at https://doi.org/10.57745/BJB0NW (Recherche Data Gouv - Original data).

## Acknowledgements

This project was supported by the Moroccan CNRST (National Center for Scientific and Technical Research) in the framework of grants URL CNRST No. 7, CNRST-FRQ/478 and RS-12. The project also received funding from the French Ministry of European and Foreign Affairs (MEAE), the French Ministry for Higher Education and Research (MESR), and the Moroccan Ministry of Higher Education, Scientific Research and Innovation (MESRSI), as part of the bilateral French – Moroccan program PHC TOUBKAL 2021 (grant number: 45858PH).

## Appendix A. Supporting information

Supplementary data associated with this article can be found in the online version at doi:10.1016/j.jhazmat.2024.135899.

## References

[1] Belloulid, M.O., 2018. National program of sanitation and wastewater treatment in morocco: objectives, achievements and challenges. Environ Water Sci Public Health Territ Intell J 67–76. https://doi.org/10.48421/IMIST.PRSM/EWASH-TI-V2I1.10956.

[2] Liu, X.-Y., Gu, X.-Y., Liu, C., Gbadegesin, L.A., He, Y., Zhang, J.-Q., 2024. Field migration of veterinary antibiotics via surface runoff from chicken-raising orchard in responding to natural rainfalls. Sci Total Environ 909, 168527. https://doi.org/10.1016/j.scitotenv.2023.168527.

[3] Zhao, X., Hu, Z., Yang, X., Cai, X., Wang, Z., Xie, X., 2019. Noncovalent interactions between fluoroquinolone antibiotics with dissolved organic matter: a $^{1}$H NMR binding site study and multi-spectroscopic methods. Environ Pollut 248, 815–822. https://doi.org/10.1016/j.envpol.2019.02.077.

[4] Zhang, D., Pan, B., 2015. Nonideal Interactions Between Organic Contaminants and Dissolved Organic Matter. In: He, Z., Wu, F. (Eds.), SSSA Spec. Publ. Soil Science Society of America, Inc, Madison, WI, USA, pp. 219–235. https://doi.org/10.2136/sssaspecpub62.2014.0042.

[5] Karwowska, B., Sperczyńska, E., 2022. Organic matter and heavy metal ions removal from surface water in processes of oxidation with ozone, UV irradiation, coagulation and adsorption. Water 14, 3763. https://doi.org/10.3390/w14223763.

[6] Piccolo, A., 1996. Humus and soil conservation. Humic Subst. Terr. Ecosyst. Elsevier,, pp. 225–264. https://doi.org/10.1016/B978-044481516-3/50006-2.

[7] Mopper, K., Stubbins, A., Ritchie, J.D., Bialk, H.M., Hatcher, P.G., 2007. Advanced instrumental approaches for characterization of marine dissolved organic matter: extraction techniques, mass spectrometry, and nuclear magnetic resonance spectroscopy. Chem Rev 107, 419–442. https://doi.org/10.1021/cr050359b.

[8] Lafrenière, M.-C., Lapierre, J.-F., Ponton, D.E., Guillemette, F., Amyot, M., 2023. Rare earth elements (REEs) behavior in a large river across a geological and anthropogenic gradient. Geochim Cosmochim Acta 353, 129–141. https://doi.org/10.1016/j.gca.2023.05.019.

[9] Carstea, E.M., Bridgeman, J., Baker, A., Reynolds, D.M., 2016. Fluorescence spectroscopy for wastewater monitoring: a review. Water Res 95, 205–219. https://doi.org/10.1016/j.watres.2016.03.021.

[10] Rodríguez-Vidal, F.J., García-Valverde, M., Ortega-Azabache, B., González-Martínez, Á., Bellido-Fernández, A., 2020. Characterization of urban and industrial wastewaters using excitation-emission matrix (EEM) fluorescence: searching for specific fingerprints. J Environ Manag 263, 110396. https://doi.org/10.1016/j.jenvman.2020.110396.

[11] Sururi, M.R., Dirgawati, M., Roosmini, D., Notodarmodjo, S., 2021. Characterization of fluorescent dissolved organic matter in an affected pollution raw water source using an excitation-emission matrix and PARAFAC. Environ Nat Resour J 19, 1–9. https://doi.org/10.32526/ennrj/19/2021008.

[12] Boukra, A., Masson, M., Brosse, C., Sourzac, M., Parlanti, E., Miège, C., 2023. Sampling terrigenous diffuse sources in watercourse: Influence of land use and hydrological conditions on dissolved organic matter characteristics. Sci Total Environ 872, 162104. https://doi.org/10.1016/j.scitotenv.2023.162104.

[13] Stedmon, C.A., Markager, S., 2005. Resolving the variability in dissolved organic matter fluorescence in a temperate estuary and its catchment using PARAFAC analysis. Limnol Oceanogr 50, 686–697. https://doi.org/10.4319/lo.2005.50.2.0686.

[14] El Hajjouji, H., Merlina, G., Pinelli, E., Winterton, P., Revel, J.-C., Hafidi, M., 2008. $^{13}$C NMR study of the effect of aerobic treatment of olive mill wastewater (OMW) on its lipid-free content. J Hazard Mater 154, 927–932. https://doi.org/10.1016/j.jhazmat.2007.10.105.

[15] Sainju, D., Lucas, R., Le Gresley, A., 2023. Evaluation of nuclear magnetic resonance spectroscopy for characterisation and quantitation of water-soluble polymers in river water. Water Res 245, 120650. https://doi.org/10.1016/j.watres.2023.120650.

[16] Zhang, L., Zhang, W., Guo, H., Shan, B., Wei, D., 2025. Characterization and function of particulate organic matter: Evidence from lakes undergoing ecological restoration. J Environ Sci 150, 91–103. https://doi.org/10.1016/j.jes.2024.03.020.

[17] Aguilar-Alarcón, P., Gonzalez, S.V., Mikkelsen, Ø., Asimakopoulos, A.G., 2024. Molecular formula assignment of dissolved organic matter by ultra-performance liquid chromatography quadrupole time-of-flight mass spectrometry using two non-targeted data processing approaches: a case study from recirculating aquaculture systems. Anal Chim Acta 1288, 342128. https://doi.org/10.1016/j.aca.2023.342128.

[18] Huang, X., Fu, X., Zhao, Z., Yin, H., 2024. The telltale fluorescence fingerprints of sewer flows for interpreting the low influent concentration in wastewater treatment plant. J Environ Manag 349, 119517. https://doi.org/10.1016/j.jenvman.2023.119517.

[19] Korshin, G.V., Sgroi, M., Ratnaweera, H., 2018. Spectroscopic surrogates for real time monitoring of water quality in wastewater treatment and water reuse. Curr Opin Environ Sci Health 2, 12–19. https://doi.org/10.1016/j.coesh.2017.11.003.

[20] Jing, Z.-B., Wang, W.-L., Nong, Y.-J., Zhu, P., Lu, Y., Wu, Q.-Y., 2022. Fluorescence analysis for water characterization: measurement processes, influencing factors, and data analysis. jwrd2022065. J Water Reuse Desalin https://doi.org/10.2166/wrd.2022.065.

[21] Hudson, N., Baker, A., Reynolds, D., 2007. Fluorescence analysis of dissolved organic matter in natural, waste and polluted waters—a review. River Res Appl 23, 631–649. https://doi.org/10.1002/rra.1005.

[22] Cohen, E., Levy, G.J., Borisover, M., 2014. Fluorescent components of organic matter in wastewater: efficacy and selectivity of the water treatment. Water Res 55, 323–334. https://doi.org/10.1016/j.watres.2014.02.040.

[23] Sgroi, M., Roccaro, P., Korshin, G.V., Greco, V., Sciuto, S., Anumol, T., et al., 2017. Use of fluorescence EEM to monitor the removal of emerging contaminants in full scale wastewater treatment plants. J Hazard Mater 323, 367–376. https://doi.org/10.1016/j.jhazmat.2016.05.035.

[24] Goffin, A., Guérin, S., Rocher, V., Varrault, G., 2018. Towards a better control of the wastewater treatment process: excitation-emission matrix fluorescence spectroscopy of dissolved organic matter as a predictive tool of soluble BOD5 in influents of six Parisian wastewater treatment plants. Environ Sci Pollut Res 25, 8765–8776. https://doi.org/10.1007/s11356-018-1205-1.

[25] EL-Nahhal, I., EL-Nahhal, Y., Mounier, S., 2023. Tracking the impact of anthropogenic inputs on fluorescent dissolved organic matter in the Gapeau River using 3D fluorescence spectroscopy. J Mar Sci Res Oceanogr 6, 139–154.

[26] A. Bouhlal, Contribution à l'étude de la valorisation du lagunage naturel par des traitements complémentaires de phytoremediation, physico-chimique et bactériologique, Thèse de doctorat, Université Moulay Ismail, Faculté des sciences, Meknès, 2018.

[27] Harshman, R.A., Lundy, M.E., 1994. PARAFAC: parallel factor analysis. Comput Stat Data Anal 18, 39–72. https://doi.org/10.1016/0167-9473(94)90132-5.

[28] Bro, R., 1997. PARAFAC. Tutorial and applications. Chemom Intell Lab Syst 38, 149–171. https://doi.org/10.1016/S0169-7439(97)00032-4.

[29] Peer, S., Vybornova, A., Tauber, J., Saracevic, E., Krampe, J., Zessner, M., et al., 2023. To analyze or to throw away? On the stability of excitation-emission matrices for different water systems. Chemosphere 333, 138853. https://doi.org/10.1016/j.chemosphere.2023.138853.

[30] Zhang, C., Mo, S., Liu, Z., Chen, B., Korshin, G., Hertkorn, N., et al., 2023. Interpreting pH-dependent differential UV/VIS absorbance spectra to characterize carboxylic and phenolic chromophores in natural organic matter. Water Res 244, 120522. https://doi.org/10.1016/j.watres.2023.120522.

[31] Weishaar, J.L., Aiken, G.R., Bergamaschi, B.A., Fram, M.S., Fujii, R., Mopper, K., 2003. Evaluation of specific ultraviolet absorbance as an indicator of the chemical composition and reactivity of dissolved organic carbon. Environ Sci Technol 37, 4702–4708. https://doi.org/10.1021/es030360x.

[32] Santos, P.S.M., Duarte, R.M.B.O., Duarte, A.C., 2009. Absorption and fluorescence properties of rainwater during the cold season at a town in Western Portugal. J Atmos Chem 62, 45–57. https://doi.org/10.1007/s10874-009-9138-1.

[33] Chang, H.-M., Vazquez, C.I., Shiu, R.-F., Chin, W.-C., 2022. Temperature effects on effluent microgel formation. Polymers 14, 4870. https://doi.org/10.3390/polym14224870.

[34] Zeeshan, M., Ali, O., Tabraiz, S., Ruhl, A.S., 2024. Seasonal variations in dissolved organic matter concentration and composition in an outdoor system for bank filtration simulation. J Environ Sci 135, 252–261. https://doi.org/10.1016/j.jes.2023.01.006.

[35] Meteoblue, Météo Ain Taoujdate, Meteoblue (2006). ⟨https://www.meteoblue.com/fr/meteo/semaine/ain-taoujdate_maroc_6546954⟩ (accessed April 29, 2024).

[36] N. AFNOR Anal De l'eau Lignes Direct pour Le Dos du Carbon Org Total (TOC) Et Le Carbon Org dissous (COD 1997.

[37] Fichot, C.G., Benner, R., 2011. A novel method to estimate DOC concentrations from CDOM absorption coefficients in coastal waters: DOC ESTIMATES FROM CDOM ABSORPTION COEFFICIENTS (n/a-n/a). Geophys Res Lett 38. https://doi.org/10.1029/2010GL046152.

[38] Miao, S., Lyu, H., Xu, J., Bi, S., Guo, H., Mu, M., et al., 2021. Characteristics of the chromophoric dissolved organic matter of urban black-odor rivers using fluorescence and UV–visible spectroscopy. Environ Pollut 268, 115763. https://doi.org/10.1016/j.envpol.2020.115763.

[39] Weishaar, J.L., Aiken, G.R., Bergamaschi, B.A., Fram, M.S., Fujii, R., Mopper, K., 2003. Evaluation of specific ultraviolet absorbance as an indicator of the chemical composition and reactivity of dissolved organic carbon. Environ Sci Technol 37, 4702–4708. https://doi.org/10.1021/es030360x.

[40] D'Andrilli, J., Silverman, V., Buckley, S., Rosario-Ortiz, F.L., 2022. Inferring ecosystem function from dissolved organic matter optical properties: a critical review. Environ Sci Technol 56, 11146–11161. https://doi.org/10.1021/acs.est.2c04240.

[41] Lee, E.-J., Lee, S.-C., Lee, K., Cha, J.-Y., Han, Y.-N., Kim, S.G., et al., 2023. Properties of river organic carbon affected by wastewater treatment plants. Sci Total Environ 858, 159761. https://doi.org/10.1016/j.scitotenv.2022.159761.

[42] Zeng, R., Mannaerts, C.M., Lievens, C., 2023. Assessment of UV–VIS spectra analysis methods for quantifying the absorption properties of chromophoric dissolved organic matter (CDOM). Front Environ Sci 11, 1152536. https://doi.org/10.3389/fenvs.2023.1152536.

[43] Zeng, R., Mannaerts, C.M., Lievens, C., 2023. Assessment of UV–VIS spectra analysis methods for quantifying the absorption properties of chromophoric dissolved organic matter (CDOM). Front Environ Sci 11, 1–12. https://doi.org/10.3389/fenvs.2023.1152536.

[44] Barreto, S.R.Giancoli, Nozaki, J., Barreto, W.J., 2003. Origin of dissolved organic carbon studied by UV-vis spectroscopy. Acta Hydrochim Hydrobiol 31, 513–518. https://doi.org/10.1002/aheh.200300510.

[45] Guo, M., Chorover, J., 2003. Transport and fractionation of dissolved organic matter in soil columns. Soil Sci 168, 108–118. https://doi.org/10.1097/00010694-200302000-00005.

[46] Ran, S., He, T., Zhou, X., Yin, D., 2022. Effects of fulvic acid and humic acid from different sources on Hg methylation in soil and accumulation in rice. J Environ Sci 119, 93–105. https://doi.org/10.1016/j.jes.2022.02.023.

[47] Jaffé, R., Boyer, J.N., Lu, X., Maie, N., Yang, C., Scully, N.M., et al., 2004. Source characterization of dissolved organic matter in a subtropical mangrove-dominated estuary by fluorescence analysis. Mar Chem 84, 195–210. https://doi.org/10.1016/j.marchem.2003.08.001.

[48] Nanaboina, V., Korshin, G.V., 2010. Evolution of absorbance spectra of ozonated wastewater and its relationship with the degradation of trace-level organic species. Environ Sci Technol 44, 6130–6137. https://doi.org/10.1021/es1005175.

[49] Wang, Q., Pang, W., Ge, S., Yu, H., Dai, C., Huang, X., et al., 2020. Characteristics of fluorescence spectra, UV spectra, and specific growth rates during the outbreak of toxic microcystis aeruginosa FACHB-905 and non-toxic FACHB-469 under different nutrient conditions in a eutrophic microcosmic simulation device. Water 12, 2305. https://doi.org/10.3390/w12082305.

[50] Luo, J., Li, S., 2021. Optical properties of dissolved organic matter in a monsoonal headwater stream, China: insights for structure, source and riverine pCO2. J Clean Prod 282, 124545. https://doi.org/10.1016/j.jclepro.2020.124545.

[51] Hansen, A.M., Kraus, T.E.C., Pellerin, B.A., Fleck, J.A., Downing, B.D., Bergamaschi, B.A., 2016. Optical properties of dissolved organic matter (DOM): effects of biological and photolytic degradation. Limnol Oceanogr 61, 1015–1032. https://doi.org/10.1002/lno.10270.

[52] Helms, J.R., Stubbins, A., Ritchie, J.D., Minor, E.C., Kieber, D.J., Mopper, K., 2008. Absorption spectral slopes and slope ratios as indicators of molecular weight, source, and photobleaching of chromophoric dissolved organic matter. Limnol Oceanogr 53, 955–969. https://doi.org/10.4319/lo.2008.53.3.0955.

[53] Clark, C.D., Bowen, J.C., de Bruyn, W.J., Keller, J.K., 2019. Optical characterization of chromophoric dissolved organic matter (CDOM) and Fe(II) concentrations in soil porewaters along a channel-bank transect in a salt marsh. Estuaries Coasts 42, 1297–1307. https://doi.org/10.1007/s12237-019-00558-6.

[54] Speetjens, N.J., Tanski, G., Martin, V., Wagner, J., Richter, A., Hugelius, G., et al., 2022. Dissolved organic matter characterization in soils and streams in a small coastal low-Arctic catchment. Biogeosciences 19, 3073–3097. https://doi.org/10.5194/bg-19-3073-2022.

[55] Lakowicz, J.R., 1999. Principles of Fluorescence Spectroscopy. Springer US, Boston, MA. https://doi.org/10.1007/978-1-4757-3061-6.

[56] H. Ba-Haddou , M. Masson , A. Daval , S.Ait Lyazidi , M. Haddad , M. Coquery , et al. , Excitation/emission fluorescence database to identify hormones, pharmaceuticals, and pesticides in environmental samples, (2024). https://doi.org/10.57745/BJB0NW.

[57] Murphy, K.R., Stedmon, C.A., Graeber, D., Bro, R., 2013. Fluorescence spectroscopy and multi-way techniques. PARAFAC. Anal Methods 5, 6557. https://doi.org/10.1039/c3ay41160e.

[58] Ishii, S.K.L., Boyer, T.H., 2012. Behavior of reoccurring PARAFAC components in fluorescent dissolved organic matter in natural and engineered systems: a critical review. Environ Sci Technol 46, 2006–2017. https://doi.org/10.1021/es2043504.

[59] Murphy, K.R., Stedmon, C.A., Wenig, P., Bro, R., 2014. OpenFluor– an online spectral library of auto-fluorescence by organic compounds in the environment. Anal Methods 6, 658–661. https://doi.org/10.1039/C3AY41935E.

[60] Ba-Haddou, H., Hassoun, H., Foudeil, S., El Bakkali, A., Ait Lyazidi, S., Haddad, M., et al., 2022. Combination of 3D Fluorescence/PARAFAC and UV–Vis Absorption for the Characterization of Agricultural Soils from Morocco. J Fluoresc 32, 2141–2149. https://doi.org/10.1007/s10895-022-03011-3.

[61] Mladenov, N., Sanfilippo, S., Panduro, L., Pascua, C., Arteaga, A., Pietruschka, B., 2024. Tracking performance and disturbance in decentralized wastewater treatment systems with fluorescence spectroscopy. Environ Sci Water Res Technol 10, 1506–1516. https://doi.org/10.1039/D3EW00671A.

[62] Sciscenko, I., Binetti, R., Escudero-Oñate, C., Oller, I., Arques, A., 2024. Dissolved organic matter behaviour by conventional treatments of a drinking water plant:

controlling its changes with EEM-PARAFAC. Appl Sci 14, 2462. https://doi.org/10.3390/app14062462.
[63] Stedmon, C.A., Bro, R., 2008. Characterizing dissolved organic matter fluorescence with parallel factor analysis: a tutorial. Limnol Oceanogr Methods 6, 572–579. https://doi.org/10.4319/lom.2008.6.572.
[64] Lorenzo-Seva, U., Ten Berge, J.M.F., 2006. Tucker's congruence coefficient as a meaningful index of factor similarity. Methodology 2, 57–64. https://doi.org/10.1027/1614-2241.2.2.57.
[65] Parr, T.B., Ohno, T., Cronan, C.S., Simon, K.S., 2014. comPARAFAC: a library and tools for rapid and quantitative comparison of dissolved organic matter components resolved by Parallel Factor Analysis. Limnol Oceanogr Methods 12, 114–125. https://doi.org/10.4319/lom.2014.12.114.
[66] Liu, B., Wu, J., Cheng, C., Tang, J., Khan, M.F.S., Shen, J., 2019. Identification of textile wastewater in water bodies by fluorescence excitation emission matrix-parallel factor analysis and high-performance size exclusion chromatography. Chemosphere 216, 617–623. https://doi.org/10.1016/j.chemosphere.2018.10.154.
[67] Flores, N., Brillas, E., Centellas, F., Rodríguez, R.M., Cabot, P.L., Garrido, J.A., et al., 2018. Treatment of olive oil mill wastewater by single electrocoagulation with different electrodes and sequential electrocoagulation/electrochemical Fenton-based processes. J Hazard Mater 347, 58–66. https://doi.org/10.1016/j.jhazmat.2017.12.059.
[68] Elmansour, T.E., Mandi, L., Hejjaj, A., Ouazzani, N., 2022. Nutrients' behavior and removal in an activated sludge system receiving Olive Mill Wastewater. J Environ Manag 305, 114254. https://doi.org/10.1016/j.jenvman.2021.114254.
[69] Helms, J.R., Stubbins, A., Perdue, E.M., Green, N.W., Chen, H., Mopper, K., 2013. Photochemical bleaching of oceanic dissolved organic matter and its effect on absorption spectral slope and fluorescence. Mar Chem 155, 81–91. https://doi.org/10.1016/j.marchem.2013.05.015.
[70] Thomas, O., Thomas, M.-F., 2017. Urban Wastewater. in: UV-Visible Spectrophotometry Water Wastewater. Elsevier,, pp. 281–315. https://doi.org/10.1016/B978-0-444-63897-7.00009-3.
[71] Guo, Y., Liu, C., Ye, R., Duan, Q., 2020. Advances on water quality detection by UV-Vis spectroscopy. Appl Sci 10, 6874. https://doi.org/10.3390/app10196874.
[72] Wang, G.-S., Hsieh, S.-T., 2001. Monitoring natural organic matter in water with scanning spectrophotometer. Environ Int 26, 205–212. https://doi.org/10.1016/S0160-4120(00)00107-0.
[73] Korshin, G.V., Li, C.-W., Benjamin, M.M., 1997. Monitoring the properties of natural organic matter through UV spectroscopy: a consistent theory. Water Res 31, 1787–1795. https://doi.org/10.1016/S0043-1354(97)00006-7.
[74] Zhang, R., Li, M., Gao, X., Duan, Y., Cai, Y., Li, H., et al., 2022. Changes in the characteristics of soil dissolved organic matter over time since inter-planting with white clover (Trifolium repens L.) in apple orchards on the Loess Plateau in China. Plant Soil. https://doi.org/10.1007/s11104-022-05697-7.
[75] Hansen, A.M., Kraus, T.E.C., Pellerin, B.A., Fleck, J.A., Downing, B.D., Bergamaschi, B.A., 2016. Optical properties of dissolved organic matter (DOM): Effects of biological and photolytic degradation. Limnol Oceanogr 61, 1015–1032. https://doi.org/10.1002/lno.10270.
[76] Holland, A., Stauber, J., Wood, C.M., Trenfield, M., Jolley, D.F., 2018. Dissolved organic matter signatures vary between naturally acidic, circumneutral and groundwater-fed freshwaters in Australia. Water Res 137, 184–192. https://doi.org/10.1016/j.watres.2018.02.043.
[77] Park, M.-H., Lee, T.-H., Lee, B.-M., Hur, J., Park, D.-H., 2009. Spectroscopic and chromatographic characterization of wastewater organic matter from a biological treatment plant. Sensors 10, 254–265. https://doi.org/10.3390/s100100254.
[78] John, R.H., Stubbins, A., Ritchie, J.D., Minor, E.C., Kieber, D.J., Mopper, K., 2009. Erratum: absorption spectral slopes and slope ratios as indicators of molecular weight, source, and photobleaching of chromophoric dissolved organic matter. Limnol. Oceanogr. 54 Limnol Oceanogr 53, 955–969. https://doi.org/10.4319/lo.2009.54.3.1023.
[79] Li, J., Wang, L., Geng, J., Li, S., Yu, Q., Xu, K., et al., 2020. Distribution and removal of fluorescent dissolved organic matter in 15 municipal wastewater treatment plants in China. Chemosphere 251, 126375. https://doi.org/10.1016/j.chemosphere.2020.126375.
[80] Stedmon, C.A., Seredyńska-Sobecka, B., Boe-Hansen, R., Le Tallec, N., Waul, C.K., Arvin, E., 2011. A potential approach for monitoring drinking water quality from groundwater systems using organic matter fluorescence as an early warning for contamination events. Water Res 45, 6030–6038. https://doi.org/10.1016/j.watres.2011.08.066.
[81] Caron, F., Sharp-King, K., Siemann, S., Smith, D.S., 2010. Fluorescence characterization of the natural organic matter in deep ground waters from the Canadian Shield, Ontario, Canada. J Radioanal Nucl Chem 286, 699–705. https://doi.org/10.1007/s10967-010-0735-x.
[82] Coble, P.G., 1996. Characterization of marine and terrestrial DOM in seawater using excitation-emission matrix spectroscopy. Mar Chem 51, 325–346. https://doi.org/10.1016/0304-4203(95)00062-3.
[83] Zheng, Y., He, W., Li, B., Hur, J., Guo, H., Li, X., 2020. Refractory humic-like substances: tracking environmental impacts of anthropogenic groundwater recharge. Environ Sci Technol 54, 15778–15788. https://doi.org/10.1021/acs.est.0c04561.
[84] Chen, M., Price, R.M., Yamashita, Y., Jaffé, R., 2010. Comparative study of dissolved organic matter from groundwater and surface water in the Florida coastal Everglades using multi-dimensional spectrofluorometry combined with multivariate statistics. Appl Geochem 25, 872–880. https://doi.org/10.1016/j.apgeochem.2010.03.005.
[85] Wu, F.C., Evans, R.D., Dillon, P.J., 2003. Separation and characterization of NOM by high-performance liquid chromatography and on-line three-dimensional excitation emission matrix fluorescence detection. Environ Sci Technol 37, 3687–3693. https://doi.org/10.1021/es020244e.
[86] Hunt, J.F., Ohno, T., 2007. Characterization of fresh and decomposed dissolved organic matter using excitation−emission matrix fluorescence spectroscopy and multiway analysis. J Agric Food Chem 55, 2121–2128. https://doi.org/10.1021/jf063336m.
[87] Diffey, B.L., 2002. Sources and measurement of ultraviolet radiation. Methods 28, 4–13. https://doi.org/10.1016/S1046-2023(02)00204-9.
[88] Singh, S., Inamdar, S., Scott, D., 2013. Comparison of Two PARAFAC models of dissolved organic matter fluorescence for a mid-atlantic forested watershed in the USA. J Ecosyst 2013, 1–16. https://doi.org/10.1155/2013/532424.
[89] Chen, G.-L., Qian, C., Gong, B., Du, M., Sun, R.-Z., Chen, J.-J., et al., 2023. Unraveling heterogeneity of dissolved organic matter in highly connected natural water bodies at molecular level. Water Res 246, 120743. https://doi.org/10.1016/j.watres.2023.120743.
[90] Quintanilla-Casas, B., Rinnan, Å., Romero, A., Guardiola, F., Tres, A., Vichi, S., et al., 2022. Using fluorescence excitation-emission matrices to predict bitterness and pungency of virgin olive oil: a feasibility study. Food Chem 395, 133602. https://doi.org/10.1016/j.foodchem.2022.133602.
[91] Ren, L.-F., Chen, R., Zhang, X., Shao, J., He, Y., 2017. Phenol biodegradation and microbial community dynamics in extractive membrane bioreactor (EMBR) for phenol-laden saline wastewater. Bioresour Technol 244, 1121–1128. https://doi.org/10.1016/j.biortech.2017.08.121.
[92] Muller, M., Milori, D.M.B.P., Déléris, S., Steyer, J.-P., Dudal, Y., 2011. Solid-phase fluorescence spectroscopy to characterize organic wastes. Waste Manag 31, 1916–1923. https://doi.org/10.1016/j.wasman.2011.05.012.
[93] ElMasry, G., Nakazawa, N., Okazaki, E., Nakauchi, S., 2016. Non-invasive sensing of freshness indices of frozen fish and fillets using pretreated excitation–emission matrices. Sens Actuators B Chem 228, 237–250. https://doi.org/10.1016/j.snb.2016.01.032.
[94] Dupuy, N., Le Dréau, Y., Ollivier, D., Artaud, J., Pinatel, C., Kister, J., 2005. Origin of French Virgin Olive Oil Registered Designation of Origins Predicted by Chemometric Analysis of Synchronous Excitation−Emission Fluorescence Spectra. J Agric Food Chem 53, 9361–9368. https://doi.org/10.1021/jf051716m.
[95] Rotich, V., Al Riza, D.F., Giametta, F., Suzuki, T., Ogawa, Y., Kondo, N., 2020. Thermal oxidation assessment of Italian extra virgin olive oil using an UltraViolet (UV) induced fluorescence imaging system. Spectrochim Acta A Mol Biomol Spectrosc 237, 118373. https://doi.org/10.1016/j.saa.2020.118373.
[96] Prempree, P., Saito, Y., Kondo, N., 2023. Characterization of time-series fluorescence properties of bean sprouts during storage using excitation emission matrix and fluorescence imaging. Spectrochim Acta A Mol Biomol Spectrosc 303, 123194. https://doi.org/10.1016/j.saa.2023.123194.
[97] Murphy, K.R., Hambly, A., Singh, S., Henderson, R.K., Baker, A., Stuetz, R., et al., 2011. Organic matter fluorescence in municipal water recycling schemes: toward a unified PARAFAC model. Environ Sci Technol 45, 2909–2916. https://doi.org/10.1021/es103015e.
[98] Sikorska, E., Khmelinskii, I., Sikorski, M., 2012. Analysis of Olive Oils by Fluorescence Spectroscopy: Methods and Applications. In: Boskou, D. (Ed.), Olive Oil - Const. Qual. Health Prop. Bioconversions. InTech. https://doi.org/10.5772/30676.
[99] Hassoun, H., Lamhasni, T., Foudeil, S., El Bakkali, A., Ait Lyazidi, S., Haddad, M., et al., 2017. Total fluorescence fingerprinting of pesticides: a reliable approach for continuous monitoring of soils and waters. J Fluoresc 27, 1633–1642. https://doi.org/10.1007/s10895-017-2100-8.
[100] Zandomeneghi, M., Carbonaro, L., Caffarata, C., 2005. Fluorescence of vegetable oils: olive oils. J Agric Food Chem 53, 759–766. https://doi.org/10.1021/jf048742p.
[101] Hassanin, H.A., 2022. Investigation on the interaction of riboflavin with aquacobalamin (Vitamin B12): a fluorescence quenching study. J Photochem Photobiol Chem 430, 113968. https://doi.org/10.1016/j.jphotochem.2022.113968.
[102] Pöhlker, C., Huffman, J.A., Pöschl, U., 2012. Autofluorescence of atmospheric bioaerosols – fluorescent biomolecules and potential interferences, Atmospheric. Meas Tech 5, 37–71. https://doi.org/10.5194/amt-5-37-2012.
[103] Edwards, A.M., 2014. Structure and General Properties of Flavins. In: Weber, S., Schleicher, E. (Eds.), Flavins Flavoproteins. Springer, New York, New York, NY, pp. 3–13. https://doi.org/10.1007/978-1-4939-0452-5_1.
[104] Santi, C.A., Cortes, S., D'Acqui, L.P., Sparvoli, E., Pushparaj, B., 2008. Reduction of organic pollutants in Olive Mill Wastewater by using different mineral substrates as adsorbents. Bioresour Technol 99, 1945–1951. https://doi.org/10.1016/j.biortech.2007.03.022.
[105] Rueda, M.P., Domínguez-Vidal, A., Llorent-Martínez, E.J., Aranda, V., Ayora-Cañada, M.J., 2024. Monitoring organic matter transformation of olive oil production residues in a full-scale composting plant by fluorescence spectroscopy. Environ Technol Innov 35, 103695. https://doi.org/10.1016/j.eti.2024.103695.
[106] Huguet, A., Vacher, L., Relexans, S., Saubusse, S., Froidefond, J.M., Parlanti, E., 2009. Properties of fluorescent dissolved organic matter in the Gironde Estuary. Org Geochem 40, 706–719. https://doi.org/10.1016/j.orggeochem.2009.03.002.
[107] Yan, P., Wei, S., Chen, Y., Ning, Q., Hu, Z., Guo, Z., et al., 2023. Fluorescence spectroscopic characterization of dissolved organic matter in the wastewater treatment plant and hybrid constructed wetlands coupling system in winter: a case study in eastern China. Environ Technol Innov 32, 103399. https://doi.org/10.1016/j.eti.2023.103399.

[108] Rodríguez-Vidal, F.J., García-Valverde, M., Ortega-Azabache, B., González-Martínez, Á., Bellido-Fernández, A., 2021. Using excitation-emission matrix fluorescence to evaluate the performance of water treatment plants for dissolved organic matter removal. Spectrochim Acta A Mol Biomol Spectrosc 249, 119298. https://doi.org/10.1016/j.saa.2020.119298.
[109] Bridgeman, J., Baker, A., Carliell-Marquet, C., Carstea, E., 2013. Determination of changes in wastewater quality through a treatment works using fluorescence spectroscopy. Environ Technol 34, 3069–3077. https://doi.org/10.1080/09593330.2013.803131.
[110] Yu, H., Song, Y., Liu, R., Pan, H., Xiang, L., Qian, F., 2014. Identifying changes in dissolved organic matter content and characteristics by fluorescence spectroscopy coupled with self-organizing map and classification and regression tree analysis during wastewater treatment. Chemosphere 113, 79–86. https://doi.org/10.1016/j.chemosphere.2014.04.020.
[111] Moslah, B., Hapeshi, E., Jrad, A., Fatta-Kassinos, D., Hedhili, A., 2018. Pharmaceuticals and illicit drugs in wastewater samples in north-eastern Tunisia. Environ Sci Pollut Res 25, 18226–18241. https://doi.org/10.1007/s11356-017-8902-z.
[112] Mostofa, K.M.G., Wu, F., Liu, C.-Q., Fang, W.L., Yuan, J., Ying, W.L., et al., 2010. Characterization of Nanming River (southwestern China) sewerage-impacted pollution using an excitation-emission matrix and PARAFAC. Limnology 11, 217–231. https://doi.org/10.1007/s10201-009-0306-4.
[113] Ayeni, T.T., Iwamoto, Y., Takeda, K., Sakugawa, H., Mostofa, K.M.G., 2022. Optical properties of dissolved organic matter in Japanese rivers and contributions to photoformation of reactive oxygen species. Sci Total Environ 826, 153671. https://doi.org/10.1016/j.scitotenv.2022.153671.
[114] Niloy, N.M., Haque, Md.M., Tareq, S.M., 2021. Fluorescent whitening agents in commercial detergent: a potential marker of emerging anthropogenic pollution in freshwater of Bangladesh. Environ Nanotechnol Monit Manag 15, 100419. https://doi.org/10.1016/j.enmm.2020.100419.
[115] Knight, E.R., Verhagen, R., Mueller, J.F., Tscharke, B.J., 2023. Spatial and temporal trends of 64 pesticides and their removal from Australian wastewater. Sci Total Environ 905, 166816. https://doi.org/10.1016/j.scitotenv.2023.166816.
[116] Coble, P.G., Green, S.A., Blough, N.V., Gagosian, R.B., 1990. Characterization of dissolved organic matter in the Black Sea by fluorescence spectroscopy. Nature 348, 432–435. https://doi.org/10.1038/348432a0.
[117] Pitta, E., Zeri, C., 2021. The impact of combining data sets of fluorescence excitation - emission matrices of dissolved organic matter from various aquatic sources on the information retrieved by PARAFAC modeling. Spectrochim Acta A Mol Biomol Spectrosc 258, 119800. https://doi.org/10.1016/j.saa.2021.119800.
[118] Guo, W., Xu, J., Wang, J., Wen, Y., Zhuo, J., Yan, Y., 2010. Characterization of dissolved organic matter in urban sewage using excitation emission matrix fluorescence spectroscopy and parallel factor analysis. J Environ Sci 22, 1728–1734. https://doi.org/10.1016/S1001-0742(09)60312-0.
[119] Ait-Lyazidi, S., Dkaki, M., Bitit, N., Meziane, D., Cazeau-Dubroca, C., Cazeau, Ph, 1998. Multiple fluorescences anomaly of 9,9′-bianthryl in solutions. Spectrochim Acta A Mol Biomol Spectrosc 55, 89–94. https://doi.org/10.1016/S1386-1425(98)00169-3.
[120] Stahlschmidt, M., Regnery, J., Campbell, A., Drewes, J.E., 2016. Application of 3D-fluorescence/PARAFAC to monitor the performance of managed aquifer recharge facilities. J Water Reuse Desalin 6, 249–263. https://doi.org/10.2166/wrd.2015.220.
[121] Slyusareva, E.A., Gerasimov, M.A., Sizykh, A.G., Gornostaev, L.M., 2011. Spectral and fluorescent indication of the acid-base properties of biopolymer solutions. Russ Phys J 54, 485–492. https://doi.org/10.1007/s11182-011-9643-y.
[122] Zhang, X.-F., Zhang, J., Liu, L., 2014. Fluorescence properties of twenty fluorescein derivatives: lifetime, Quantum Yield, Absorption and Emission Spectra. J Fluoresc 24, 819–826. https://doi.org/10.1007/s10895-014-1356-5.
[123] Lamhasni, T., El-Marjaoui, H., El Bakkali, A., Lyazidi, S.A., Haddad, M., Ben-Ncer, A., et al., 2019. Air pollution impact on architectural heritage of Morocco: Combination of synchronous fluorescence and ATR-FTIR spectroscopies for the analyses of black crusts deposits. Chemosphere 225, 517–523. https://doi.org/10.1016/j.chemosphere.2019.03.109.
[124] Sanli, G., Celik, S., Joubi, V., Tasdemir, Y., 2023. Concentrations, phase exchanges and source apportionment of polycyclic aromatic hydrocarbons (PAHs) In Bursa-Turkey. Environ Res 232, 116344. https://doi.org/10.1016/j.envres.2023.116344.
[125] Tang, J., Li, X., Luo, Y., Li, G., Khan, S., 2016. Spectroscopic characterization of dissolved organic matter derived from different biochars and their polycyclic aromatic hydrocarbons (PAHs) binding affinity. Chemosphere 152, 399–406. https://doi.org/10.1016/j.chemosphere.2016.03.016.
[126] Li, Y., Li, A.-M., Xu, J., Li, W.-W., Yu, H.-Q., 2013. Formation of soluble microbial products (SMP) by activated sludge at various salinities. Biodegradation 24, 69–78. https://doi.org/10.1007/s10532-012-9558-5.
[127] He, W., Chen, M., Schlautman, M.A., Hur, J., 2016. Dynamic exchanges between DOM and POM pools in coastal and inland aquatic ecosystems: A review. Sci Total Environ 551–552, 415–428. https://doi.org/10.1016/j.scitotenv.2016.02.031.
[128] Goldman, J.H., Rounds, S.A., Needoba, J.A., 2012. Applications of fluorescence spectroscopy for predicting percent wastewater in an urban stream. Environ Sci Technol 46, 4374–4381. https://doi.org/10.1021/es2041114.
[129] Mailler, R., Gasperi, J., Coquet, Y., Derome, C., Buleté, A., Vulliet, E., et al., 2016. Removal of emerging micropollutants from wastewater by activated carbon adsorption: experimental study of different activated carbons and factors influencing the adsorption of micropollutants in wastewater. J Environ Chem Eng 4, 1102–1109. https://doi.org/10.1016/j.jece.2016.01.018.
[130] Rhenifel, M., Bouftila, O., Bouhaddioui, A., Karkouri, A.El, Bahhou, J., 2020. Wastewater treatment efficiency by natural lagooning in new station of aïn chiffa at sefrou city-Morocco. Bull Inst Sci Sect Sci Vie 42, 43–50, 8.
[131] Cheng, Y., Cheng, Q., Zhao, C., Ren, X., Wang, Y., Kou, Y., et al., 2023. Evaluation of efficiently removing secondary effluent organic matters (EfOM) by al-based coagulant for wastewater recycling: a case study with an industrial-scale food-processing wastewater treatment plant. Membranes 13, 510. https://doi.org/10.3390/membranes13050510.